Physics – Uspekhi **63** (7) 648 – 667 (2020)

REVIEWS OF TOPICAL PROBLEMS PACS numbers: 71.38.Ht, **73.63. – b**, **79.70. + q**

Field emission from carbon nanostructures: models and experiment

E D Eidelman, A V Arkhipov

DOI: https://doi.org/10.3367/UFNe.2019.06.038576

Contents

Abstract. Models of field (cold, autoelectron) emission from various types of carbon nanostructures, other than graphene, are described. The experimental results are compared with theoretical predictions.

Keywords: carbon nanostructures, field emission properties, field emission models, emission threshold, emitters, cathodes for emission devices

1. Introduction. Fowler–Nordheim law

Although cathodes for thermoelectronic emission still retain dominant positions in vacuum electronics, it is generally accepted that cold cathodes for field (cold, autoelectronic) emission can have a number of fundamental advantages, such as higher efficiency and a short turn-on time. The disadvantages of cold cathodes are the difficulty of obtaining high emission currents and the insufficient service life under conditions of a technical vacuum. The field-emission data set in the general case and for field (cold, autoelectronic) emission from carbon nanostructures (CNSs) consists of volt-ampere characteristics measured under different conditions. Usually, the threshold electric field E_t is determined, which represents the electric field strength averaged over the field gap and corresponds to the appearance of the minimal emission current, as a rule, of about 1 nA.

In experiments, the current I flowing in the circuit is measured as a function of the voltage U applied to the anode–cathode gap. It is commonly assumed that this dependence can be described by the Fowler–Nordheim (FN) law [1]

$$j = A\,\frac{E^2}{\varphi}\,\exp\left(-\frac{B\varphi^{3/2}}{E}\right). \tag{1}$$

This equation relates the emission current density j to the external electric field strength E; φ is the electron work function of the cathode material. The rest of the quantities entering the FN equation are expressed in terms of universal constants:

$$A = \frac{e^3}{16\pi^2\hbar} \cong 2.6\times 10^{-24}\ [\mathrm{C\ \Omega^{-1}}]\,,$$
$$B = \frac{4}{3}\,\frac{\sqrt{2m}}{\hbar e} \cong 1.1\times 10^{38}\ [\mathrm{J^{-1/2}\,C^{-1}\,m^{-1}}]\,. \tag{2}$$

Here, e and m are the electron charge and mass, respectively, and $\hbar$ is Planck's constant. For very high field strengths, A and B also contain functional factors [2]. However, they can be ignored in CNS experiments.

The FN equation is derived in the one-dimensional approximation, i.e., the vacuum boundary of an emitter is assumed flat and the electric field E is assumed uniform. The field emission current is determined by integrating the contributions of electrons in the emitter volume with different energies ε:

$$I(E) = \frac{e}{2\pi\hbar}\int_{-\infty}^{\infty} n(\varepsilon)D(\varepsilon, E)\,\mathrm{d}\varepsilon\,. \tag{3}$$

Here, $n(\varepsilon)$ is the energy density of occupied electronic states described by the Fermi function, and $D(\varepsilon, E)$ is the transpar-

E D Eidelman [1, 2, *], **A V Arkhipov** [2]
[1] Ioffe Institute,
ul. Politekhnicheskaya 26, 194021 St. Petersburg, Russian Federation
[2] Peter the Great St. Petersburg Polytechnic University,
ul. Politekhnicheskaya 29, 195251 St. Petersburg, Russian Federation
E-mail: [*] Eidelman@mail.ioffe.ru

Received 16 April 2019, revised 31 May 2019
Uspekhi Fizicheskikh Nauk **190** (7) 693 – 714 (2020)
Translated by M N Sapozhnikov; edited by V L Derbov

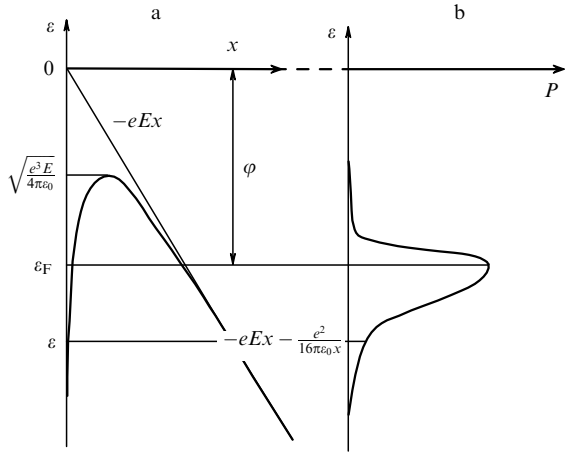

Figure 1. (a) Typical energy level diagram and (b) calculated energy distribution $P(\varepsilon)$ of emitted electrons for a metal in an applied external field E. The emitting surface ($x = 0$) separates the metal ($x < 0$) from a vacuum ($x > 0$). The surface barrier shape for an electron (with charge e) is determined by the contribution eEx of the external field and the potential $e^2/(16\pi\varepsilon_0 x)$ of mirror-image forces (ε_0 is the vacuum permittivity). ε_F is the Fermi energy, φ is the work function, $\sqrt{e^3E/(4\pi\varepsilon_0)}$ is the barrier energy, small compared to ε_F, in fact, for all real field strengths.

ency of the surface barrier for electrons with energy ε. The surface barrier in pioneering paper [1] was acute-angled with the potential eEx. In [3, Ch. 6], the contribution of the mirror-reflection force potential of $e^2/(16\pi\varepsilon_0 x)$ is taken into account (Fig. 1a). The calculation is performed for temperature $T = 0$. In this case, the Schrödinger equation is written in the form

$$\begin{aligned} &\frac{\mathrm{d}^2\psi}{\mathrm{d}x^2}+\frac{2m}{\hbar^2}\left[\varepsilon-(-w)\right]\psi=0\,, && x<0\,,\\ &\frac{\mathrm{d}^2\psi}{\mathrm{d}x^2}+\frac{2m}{\hbar^2}\left[\varepsilon-\left(-eEx-\frac{e^2}{16\pi\varepsilon_0 x}\right)\right]\psi=0\,, && x>0\,. \end{aligned} \tag{4}$$

The energy w corresponding to the bottom of the filled band is also discussed in [3]. The use of approximations and procedures mentioned above gives the emission dependence in the form of (1).

The FN law for macroscopic metal cathodes has been confirmed in many experiments [3, Ch. 2]. At the same time, for other types of emitters (e.g., semiconducting [2, 4, 5]), more or less significant deviations of emission characteristics from the FN law can be observed, which are related to the peculiarities of their electronic properties, in particular, to the form of the density of states $n(\varepsilon)$. Additional peculiarities appear in the case of emission from spikes about several nanometers in size. If the spike radius is comparable to the thickness of the surface barrier in the tunneling problem, the determination of the electric field strength, unlike the one-dimensional case, becomes ambiguous.

The situation considerably changed after the discovery of carbon nanotubes (CNTs) and their capability for field emission at comparatively low applied voltages [6, 7]. Such a capability was found even somewhat earlier for carbon fibers similar to CNTs [8, 9].

The next step in the same direction is the move to a completely or almost completely planar system which, due to the increase in the area of the emitting region, could have an even higher thermal and mechanical stability and stability against sputtering caused by ion bombardment. However, the move to a planar structure inevitably reduces the amplification coefficient of the applied external electric field, which raises a question about the fundamental possibility of 'low-voltage' field emission (with a low threshold voltage) in such ax system.

Nevertheless, numerous examples [10–23] of materials and structures already known for a few decades demonstrate their capacity for emission with a low threshold voltage in the case of a relatively smooth emitting surface not containing, at least at first glance, elements with a high aspect ratio (length-to-width ratio). We will call such materials carbon nanostructures. A separate material is graphene, which we will not consider here.

Most CNSs are either purely carbon or contain a great amount of carbon. The typical feature of such materials is the presence of nanosize regions in their structure — grains with drastically different electrical and thermophysical properties typical of the two main allotropic forms of carbon. Graphite-like regions contain carbon predominantly in the sp^2 hybridization state and, like graphite, have considerable electrical and thermal conductivities and comparatively low specific heat capacity. Diamond-like carbon (DLC) regions, both amorphous and consisting of crystallites, are composed of carbon atoms in the sp^3 state. They, like diamond, have the electronic structure of a wide-bandgap semiconductor or a dielectric and low electric conductivity, but a rather high heat capacity.

In this review, we compare the advantages and disadvantages of various models of the field emission of electrons from CNSs, both traditional and new ones. The review is organized as follows.

In Section 2, the features of emission from CNS materials observed in experiments are presented.

In Sections 3 and 4, we analyze the main theoretical models proposed to date, both traditional, widely used (Section 3) and recently proposed and not generally accepted so far (Section 4). The correspondence between all models and experimental data is assessed. The main attention is focused exactly at new nontraditional models.

Models, in which the agreement between theory and experiment is achieved by introducing fitting parameters that have no clear physical meaning are excluded from consideration.

Conclusions are presented in the final Section 5, where the summary table demonstrates the correspondence between experimental data and model calculations.

2. Features of field emission from carbon nanostructures

2.1 Emission centers

One of the important circumstances that should be taken into account in any model of electron emission from CNSs is the spatial inhomogeneity of CNS materials. Many experimental results (e.g., [10, 14, 24–26]) suggest that electrons are emitted into a vacuum not from the whole surface of a cathode but from separate small regions containing carbon in the sp^2 hybridization state. These small regions emitting electrons are called emission centers (ECs).

The necessity of the presence of sp^2 carbon in CNS ECs is obvious: the transport of electrons to the emitting region can occur only through regions with nonzero electric conductivity.

One of the reliable experimental proofs of the EC smallness is presented in paper [27], whose authors compared the emission properties of a cathode made of silicon spikes covered with DLC films with thickness h varied from 0.1 to 2.4 μm. The static characteristics of emission were determined during the flow of a weak emission current (no more than 10^{-5} A) from the cathode under study to an anode with a smoothed surface located at a small distance (50–200 μm) from the characterized spike. Note that CNS films always contain regions with the sp^3 hybridization of carbon atoms (in nanodiamond and diamond-like films, such regions dominate) and graphite-like regions with the sp^2 hybridization. For purely silicon spikes, the threshold field strength — the ratio of the applied voltage to the vacuum gap width between the cathode and anode at which the emission current appears — proved to be considerably higher than for the same spikes covered with a DLC film. This made it possible to associate the increased emission activity precisely with the presence of the coating. Note that the threshold field for coated spikes was independent, in fact, of the coating thickness. An analysis of emission characteristics shows that the emission current is restricted by the ohmic resistance R of a carbon film itself. The dependence of this quantity on the coating thickness h proves to be directly proportional, $R/h \cong$ const. These facts allow conclusions on the emission spectrum shape.

The proportional dependence can be readily explained assuming that for any coating thickness the emission occurs from the same number of local centers on its surface, possibly from the only center. In this case, the electric resistance restricting the emission current will indeed be directly proportional to the length h of a channel conducting the current through the coating. Such current channels can be identified with conducting sp^2 boundaries between the diamond-like regions of a nonostructured film.

The independence of the threshold field from the emitter surface area suggests that the size d of the EC is small ($d \ll h$) and the local amplification of the field (see below Section 3.1.1) in its vicinity is determined namely by its size d. Since the minimal coating thickness in these experiments was $h = 0.1$ μm, the EC size does not exceed a few dozen nanometers.

This conclusion is confirmed for many other types of CNSs by direct microscopic observations presented, for example, in Refs [13, 14, 28–31] for structured CNS films with different phase ratios sp^2/sp^3. The spatial distributions of the emission current were measured in [13, 14, 29, 30] with a modified or standard tunneling microscope. In [28–31], emission distributions with a lower spatial resolution were obtained by directing emitted electrons onto a luminescent screen and observing optical microimages.

Thus, the existence of emission centers and concentration of the emission current in ECs — small regions of the vacuum boundary different in their properties from the rest of the surface — are the first experimental facts that should be taken into account in the formulation and estimates of emission models for CNSs of this type.

2.2 Relation between emission properties and the composition and structure of a material

A question arises as to the existence of the optimal relation of the amounts of sp^2 and sp^3 carbon. However, the proportion of the sp^2 phase called optimal by different authors varies in a broad range from 5% [32], 17% [33], 23% [13], to 1/3 [34], etc. At the same time, it is known that materials containing almost 100% sp^2 carbon can also have good emission properties. This is confirmed by results [11, 25, 31, 35–41] obtained with films consisting of graphite-like nanosize regions in which the emission threshold was observed for fields of about a few units of V μm^{-1}.

In most of these experiments, the current emission dependences in a static electric field were determined by standard methods, which makes possible a quantitative comparison of the results. CNS cathodes with a flat surface and areas from several mm^2 to several cm^2 were used. The electric field was produced in a gap a few to hundreds of micrometers in width, allowing the use of relatively low electric voltages. The anode was ether flat and located parallel to the cathode or cylindrical with a flat or rounded end. The anode area was chosen smaller than that of the CNS, which prevented the uncontrollable amplification of the electric field by the sharp edges of the cathode. Because the field amplification by the individual elements of the CNS is unknown, the emission ability of the CNS was estimated from the average electric field strength between the anode and cathode.

Conditions under which graphite-like CNS films with a smooth vacuum boundary can emit electrons with a low emission threshold were studied in experiments [42–45] with thin, 1–2-nm-thick films, analyzing their structure by surface-sensitive methods. It was found that emission in fields with strengths from fractions of to a few V μm^{-1} can occur only for discontinuous coverings consisting of separate nanosize sp^2 carbon islets that have no ohmic contacts between them or with a substrate. These islets are similar to sp^2 clusters which are regarded as the emission centers of DLC films (see Section 4.3.3 below).

Similar clusters are one of the structural elements of many carbon nanomaterials emitting in weak fields or can be present there as impurities. They include nanocluster diamond-graphite films [30, 46–50] and composites [13, 33, 51–54], detonation nanodiamonds [19, 55] and their graphitization products [48, 52], different types of nanoporous carbon [56–58], and composition structures with a high concentration of boundaries between sp^2 and sp^3 carbons and vacuum (e.g., structures consisting of carbon fibers or CNTs and nanodiamonds [59–61]).

As a whole, the high emission ability of carbon materials caused by their inhomogeneity, the 'porous' structure, and the high concentration of boundaries separating regions with contrasting physical properties is the next experimental fact accepted by most researchers. A less reliable and universal experimental observation is the conclusion that the necessary structural element of the low-voltage emission center is an isolated region with dominating sp^2 carbon.

2.3 Emission current and the work function of carbon nanostructures

Assume that the FN law (1) is valid for each individual emission CNS center, so that $j = j_c$ is the current density produced by one EC with area S_c. In experiments, the current from many ECs is measured. We denote their number on a surface with area S by N_c. Then, the total current is

$$I = jS = N_c j_c S_c \,. \tag{5}$$

Of course, formula (5) is valid only for identical emitting regions. In reality, the exponential dependence of the emis-

sion current on the particular composition and geometrical features of the emitting region leads to a scatter in the emission current from different regions by several orders of magnitude. Therefore, relation (5) is the result of some averaging. However, this averaging does not affect the further discussion.

It is convenient to analyze experimental data using the average current density obtained from a combination of Eqns (5) and (1) [32]:

$$j = AN_c \frac{S_c}{S} \frac{E^2}{\varphi} \exp\left(-\frac{B\varphi^{3/2}}{E}\right). \quad (6)$$

Expression (6) is commonly used, often implicitly, to describe emission from CNSs. The use of this law obviously assumes that the field strength E near each EC is the same, although this assumption can be incorrect in real experiments. The results of direct measurements of current dependences for individual ECs are compared in [62, 63].

Often, when presenting experimental data, instead of the field strength E in formula (6), the value of the applied voltage U is used, and the proportionality coefficient between them is considered included in A and B. Of course, in this case, A and B are no longer universal constants and, strictly speaking, are not constant at all.

It is the uncertainty in the electric field strength E used in the quantitative description that provides good agreement with experiments by replacing universal world constants A and B in (2) by polynomials in E, thereby introducing the required number of fitting parameters. It is unlikely that such an approach can be used to obtain qualitative, physically clear results.

Expression (6) will be considered below as a law characterizing a set of some averaged ECs. It can be rewritten as

$$\ln\left(\frac{j}{E^2}\right) = \ln\left(\frac{A}{\varphi}\right) + \Gamma - \frac{B\varphi^{3/2}}{E}. \quad (7)$$

Here, $\Gamma = \ln(N_c S_c/S)$. The dependence $y(x)$, where $y = \ln(j/E^2)$, $x = 1/E$ (i.e., the dependence of $\ln(j/E^2)$ on $1/E$), is called the emission characteristic in the FN coordinates. One can easily see that relation (7) gives the straight line $y(x) = y_0 - bx$ with the slope $b = B\varphi^{3/2}$ intersecting with the vertical axis at $y_0 = \ln(A/\varphi) + \Gamma$.

The parameter Γ is related to quantities poorly determined in experiments: the number N_c of ECs and the EC area S_c [32]. Because of this, it is rarely used in analyses of CNS experimental data. However, such attempts were described, e.g., in [64, 65]. The coefficient b is defined better, and the slope in the FN coordinates is used by almost all researchers to determine the 'effective' work function $\varphi = \varphi_c$ from measured current dependences. This is facilitated by the fact that experimental curves $j(U)$ are often approximately linear in the FN coordinates, at least for some intervals of applied voltages.

The main feature and problem of applying such an approach to CNSs of these types is the great difference between the effective work function determined by emission characteristics and its values obtained by other methods.

One of the earlier studies in which both these values were determined was paper [10], where the emission properties of nitrogen-containing DLC films with smooth surfaces were investigated. The value of φ_c determined from the form of field emission characteristics assuming the absence of the local amplification of the applied field (see Section 3.1) was 0.12–0.16 eV. To measure the work function by an independent method, the field emission energy distribution (FEED) was measured for electrons during laser irradiation of a sample with the simultaneous detection of the photoelectric and field emission currents. One of the two observed peaks of the FEED was formed by electrons tunneling through a surface barrier with energies near the Fermi level. The second peak was formed by photoelectrons escaping to the vacuum 'above' the surface barrier. Their minimal energy corresponded to the position of the peak top. The difference between the Fermi and vacuum levels determines the 'real' work function of the DLC, estimated as 4.9 eV. Similar values of the 'photoelectron' work function φ were obtained by the same method for diamond films ($\varphi \approx 6$ eV [26]) and nanocrystalline graphite ($\varphi \approx 4.0-4.2$ eV [66]).

The work function of carbon emitters was also independently measured by the contact potential difference method, giving — with the use of an atomic-force microscope — the local values of the surface potential. It was found that $\varphi \approx 4.7$ eV. This method gave $\varphi \approx 4.9$ eV for DLC films with different degrees of nitrogen doping [67]. In [44, 45], the same value $\varphi \approx 4.7$ eV for island-structure graphite-like carbon films was obtained by the photoelectric method and the contact potential difference method, respectively. In all these cases, the low-threshold field emission was observed and the slopes of the FN characteristics corresponded to φ_c of about 0.1 eV or smaller.

A considerable difference (by tens or hundreds of times) between the 'effective' work function determining the characteristics of field emission for CNSs of many types and the work function of 4–5 eV measured for carbon by all alternative methods is one of the experimental facts requiring an explanation in any models of field emission from CNSs.

2.4 Dynamics of emission processes: correlations and hysteresis

Phenomena considered in Sections 2.1–2.3 are usually observed in field-emission studies and are always taken into account in the construction of models. The dynamics of emission processes — correlations and hysteresis of emission currents — only recently attracted the attention of researchers (see [68–73]). These phenomena can substantially determine the choice of the adequate emission model for CNSs. Therefore, correlations and hysteresis of emission currents will be considered in more detail than the work function, the relation between emission properties and the composition and structure of a material, and the existence of ECs. We will show how experimental data can be used to obtain information important for the construction of the CNS emission model.

It is known that the current of carbon cathode emitters is often unstable and its value can change intermittently when a constant voltage is maintained between the cathode and anode. Regular 'blinkings' corresponding to the switching on and off of individual emitting regions are observed [31]. The method of statistical processing of time dependences of field emission currents is discussed in paper [68] and references therein. Papers [69–71] contain examples of practical applications of such data. The authors of these papers performed the correlation analysis of oscillograms of emission currents from limited regions of the surface of fullerene-containing [69] and nanoporous [70, 71] carbon

measured in an electrostatic field. Analysis demonstrated the nonrandom character of current fluctuations and their relation to fields inside a CNS cathode.

In [71], aside from correlations of fluctuations of emission currents from the same region, the mutual correlation of currents from different regions of a nanoporous carbon cathode was also studied. It was shown that current jumps corresponding to blinkings of the emission pattern do not occur simultaneously or instantly: the process propagates over the cathode surface with a fairly low velocity, on the order of a few tens or hundreds of m s^{-1}. This result is inconsistent with the concept of field emission as an inertionless process.

In [72, 73], the dynamics of emission processes in nanocarbon cathodes was studied in a more direct way. The time dependences of the emission current were recorded by applying voltage pulses to a planar field gap separating the anode from the macroscopically flat surface of a CNS sample. The main experimental problem was the separation of the capacitance (induced) and electronic components of the measured current. This problem was successfully solved using a specially developed instrument and specially developed measurement methods [71]. Despite a rather long duration of voltage pulses (from several to hundreds of microseconds), two of the materials studied, nanoporous carbon [71–75] and multilayer fulleroid films [71–74], demonstrated a considerable hysteresis of emission characteristics manifested in an increase in the emission capacity during the pulse (Fig. 2a). As a result, the back branch of the current curve measured during field decay was located higher and had a smaller slope than the direct branch in the FN coordinates (Fig. 2c). The correctness of these measurements is confirmed by the fact that the hysteresis was not observed for cathodes of other types, in particular, the CNT cathode [71].

The hysteresis of emission currents is commonly explained (see [40, 76–78]) by emitter heating, the removal of absorbed layers from the surface, or the structural rearrangement of emitting regions. Studies [71–75] of the evolution of current dependences on parameters and the field pulse shape (Fig. 3a) gave results that cannot be explained by factors mentioned above (Fig. 3b). Experiments with double field pulses (Figs 2a, b) showed that the 'memory' of the emitting structure about the achievement of an activated state can be maintained for a long time, tens or hundreds of microseconds. However, it is rapidly lost on proceeding from the field decay to its growth (Fig. 2b). After statistical processing of the temporal characteristics of field emission currents, these phenomena are clearly observed in qualitative dependences in Figs 2c and 3c.

Thus, experimental studies of the hysteresis and correlations of emission currents at the microsecond scale in CNSs require its explanation in the field emission models discussed here.

2.5 Energy distribution of emitted electrons

As mentioned above, one of the main problems in the study of the mechanism of electron emission from cathodes of the type investigated is that many of the experimental methods used give only averaged parameters of the CNS surface, whereas the emission current comes from ECs with a small total area whose properties are obviously different from averaged values. This determines the special value of the data that can be obtained when studying the energy distributions of emitted electrons, since these distributions reflect precisely the properties of directly emitting regions and structures.

For the simplest one- dimensional case of emission from a conductor, the theory predicts an FEED like (see [79] and references therein and also Fig. 1b)

$$P(\varepsilon) = 2P_{\mathrm{F}} \frac{\exp\left(\Delta/\delta\right)}{1+\exp\left(\Delta/k_{\mathrm{B}}T\right)} \,. \tag{8}$$

Here, k_{B} is the Boltzmann constant, T is the electron temperature, and $\Delta = \varepsilon - \varepsilon_{\mathrm{F}}$ is the deviation of the emitted electron energy ε from the Fermi energy ε_{F}. The distribution function P itself is defined, as usual, by the relation

$$\mathrm{d}j(\varepsilon) = P\,\mathrm{d}\varepsilon \,. \tag{9}$$

The constant P_{F} is the maximum of the distribution function for electrons emitted from the Fermi level $P_{\mathrm{F}} = P(\varepsilon_{\mathrm{F}})$. The parameter

$$\delta = \frac{1}{2}\frac{\hbar e}{\sqrt{2m}}\frac{E}{\varphi^{1/2}} \tag{10}$$

is determined by the relation between the external field strength E and the work function φ.

Details of the derivation of these relations can be found in monograph [3, Ch. 8]. The distribution law (8) allows using experimental data on the FEED for independent estimates of temperature and the local field strength for an emitting region. The correctness of this law for metals was confirmed in many experiments (see, e.g., [3, Ch. 14, 15] and [80]).

Although FEED measurements are very informative, the number of experimental studies containing such data is relatively small because of the complexity of measurements. Electrons emitted from a cathode or from part of it should be extracted from the gap between the cathode and anode with the help of a grid electrode and directed to an energy analyzer. Decelerating-field analyzers are commonly used. A small value and the time instability of emission currents from CNSs prevents a FEED measurement with the required resolution, the typical resolution being from 10 to 50 meV. These difficulties increase if the cathode has a low conductivity, which is typical for CNS cathodes. As a result, the potentials of different ECs can be substantially different. In this case, it is necessary to analyze electrons emitted by an individual EC using a movable analyzer with a small entrance hole.

Only a few FEED studies for CNSs are known, where the results were used to measure the effective temperature of ECs based on law (8). In [81], such an estimate was performed for CNTs and in [82] for DLC films based on experiments [83]. In both cases, the effective temperature was measured to be about 2000 K or slightly lower.

Since substrates in all experiments discussed were at room temperature, the temperature difference between the surfaces of CNS films was no less than 1500 K. For films of about 50 nm in thickness [83], the temperature gradient should be about 30 K nm^{-1}. For ECs of about 5 nm in size, the gradient would be as large as hundreds of degrees per nanometer, even taking into account the peculiarities of the temperature distribution between regions with sp^2 and sp^3 hybridized carbon atoms [82]. Such results are rather suspicious. Note that, during field emission from a metal, the surface of emitters not only is not heated (see [84]), but can even be cooled [80].

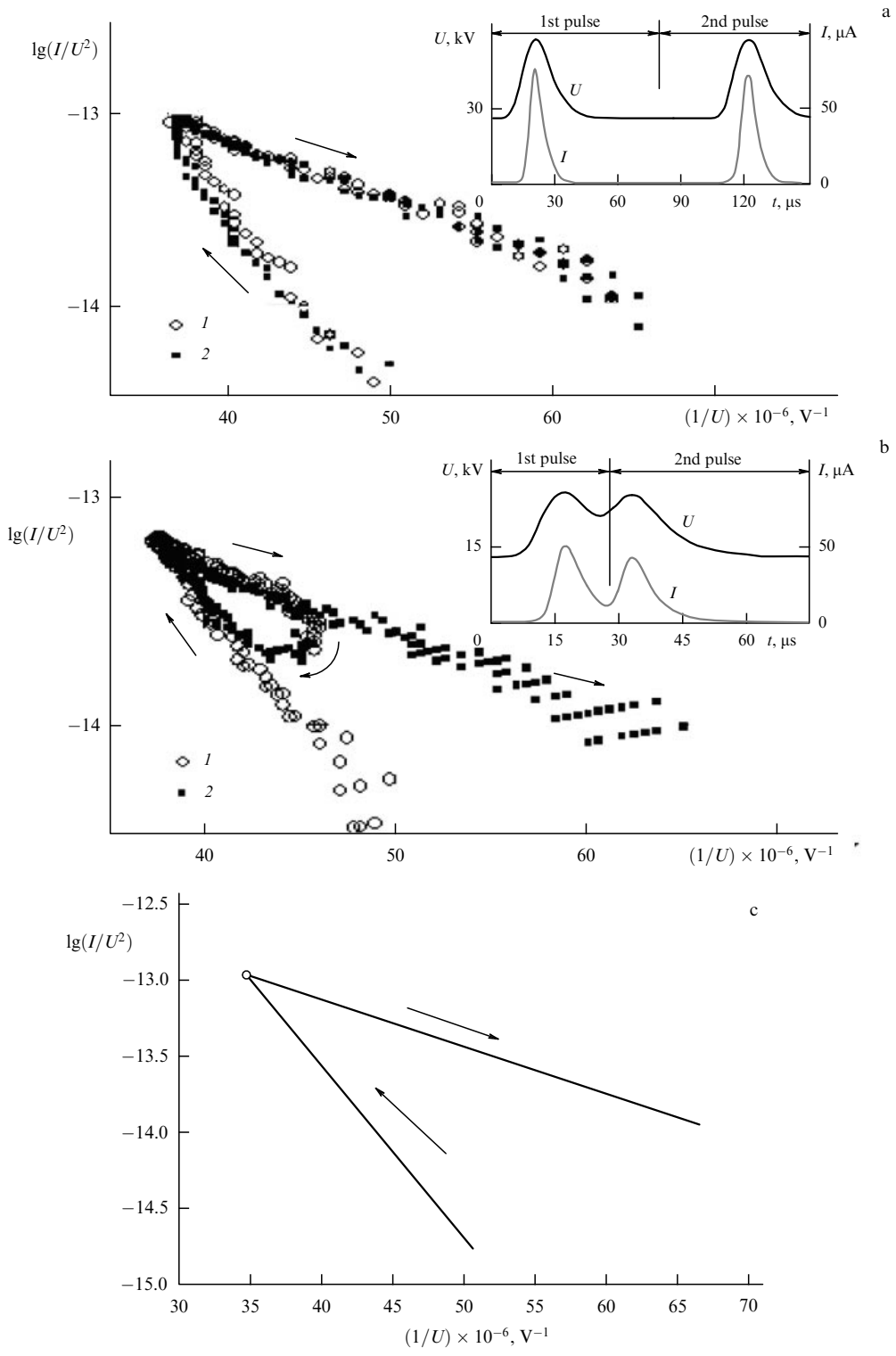

Figure 2. Hysteresis of the emission characteristics of a nanoporous carbon sample measured using double voltage pulses [71, 72]. The time delay between pulses was (a) 100 μs and (b) 20 μs (shorter than the pulse duration). (c) Qualitative picture of the hysteresis. Typical FN 'straight lines' when applying external voltage pulses constructed by approximation of the measurement results after the statistical processing of data presented in Fig. 2b. The arrows show the directions of the voltage increase and decrease in a pulse.

Estimates from the heat conduction equation show that the heating by the current to hundreds or even a thousand degrees Kelvin is possible. Indeed, it is known that the stationary thermal regime is established in graphite for the time Δt of about $10^{-4}-10^{-5}$ s [80]. Then, the temperature can be estimated from the Fourier equation by disregarding the heat conduction as

$$T=\frac{j\Delta t}{\sigma\rho C}\,. \tag{11}$$

Estimates are made using data from paper [85], where currents j for individual spikes were measured to be about

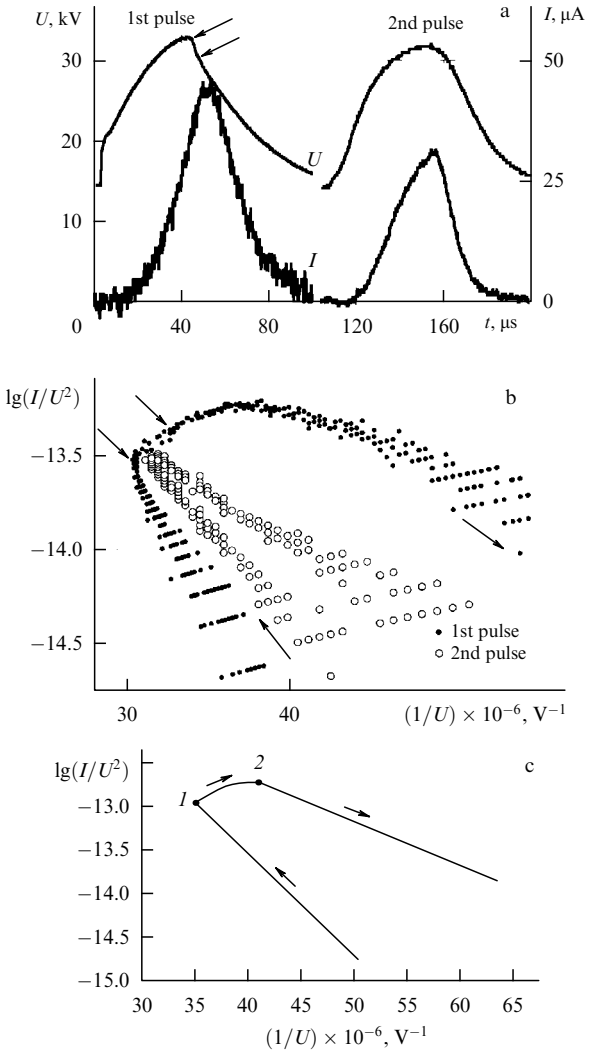

Figure 3. (a) Voltage pulses of different shapes and (b) the emission characteristics of a nanoporous carbon sample with a hysteresis measured with the help of these pulses [71, 73]: 1st pulse with the rapid decay part (shown by arrows); 2nd 'smooth' bell-like pulse. (c) Qualitative picture of the hysteresis obtained as in Fig. 2 but between FN 'straight lines' the characteristic increases in the *1–2* region.

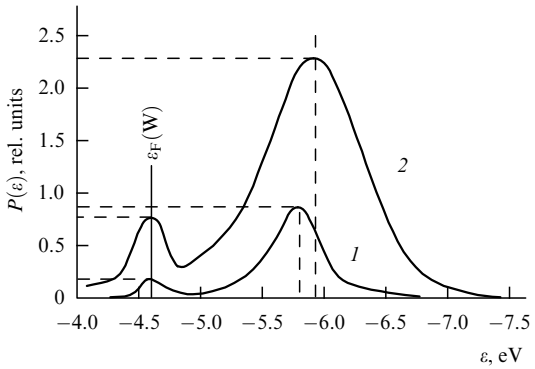

Figure 4. FEED approximations using the results of measurements [83] for low (0.4 kV) (*1*) and high (2.6 kV) (*2*) applied external voltages. The first peak (on the left) corresponds to emission from a tungsten substrate (Fermi energy $\varepsilon_F = 4.6$ eV), and the second peak corresponds to emission from a 100-nm diamond-like film.

100 mA cm^{-2} or higher. Assuming that the EC size is, at least, 20 times smaller than that of the spike (the spike size is ≈ 100 nm [85]), we obtain $j \approx 40$ A cm^{-2}. By estimating EC characteristics from the tabulated graphite parameters: density $\rho \approx 2$ g cm^{-3}, heat capacity $C \approx 0.1$ J kg^{-1} K^{-1}, and electric conductivity $\sigma \approx (3-12) \times 10^4$ Ω^{-1} m^{-1}, we obtain $T \approx 10^2 - 10^3$ K. This estimate corresponds to measurements [81, 83].

However, no heat conduction mechanism can explain such high temperature differences following from FEED measurements in CNS films.

A number of experiments gave results qualitatively different from the FN law (Fig. 1b), indicating the existence of a different emission mechanism. The emission properties of DLC coatings deposited on metal spikes are presented in [83, 86, 87]. The FEED spectra exhibit a broad (more than 1 eV) peak shifted upon varying the applied field strength. In the case of thin coatings, a narrow peak near the Fermi level of the metal is also present (Fig. 4). A spectral distribution of this type does not correspond to a simple FN emission model. It can suggest the penetration of the field into the emitter volume and the formation of a gas of nonequilibrium 'hot' electrons, which determine the enhanced emission ability. Similar FEED spectra were also obtained for sp^3 carbon films on flat substrates [28, 88].

Note that the assumption itself about the electric-field penetration into the emitter volume seems rather natural for poorly conducting materials based on sp^3 carbon. However, FEED spectra with a broad low-energy peak were also obtained for CNSs containing carbon mainly in the sp^2 state. For example, such spectra were measured for nanographite films [89]. Note that, as far as we know, the qualitative dependence of the FEED spectrum on the emission current was first directly observed in [89]. The low-current spectrum agrees with the classical FN theory of field emission and exhibits a single peak about 0.2 eV in width located near the Fermi level. For currents above 300 nA, the peak is split into two, one of the peaks shifts, and the spectrum becomes similar to that in Fig. 4. This observation allows us to resolve the contradiction between the results presented in earlier publications.

The fact that the shape of FEEDs obtained in experiments does not always correspond to the FN emission model should also be taken into account in the construction of a field emission model for CNSs.

3. Models of field emission from materials with carbon nanostructures

3.1 Field concentration model: model with the β factor

3.1.1 Description of the field concentration model. One of most natural explanations of the capability of carbon materials for low-voltage electron emission could be the presence of elements concentrating the applied electric field (Fig. 5), for example, spikes on the surface, carbon nanotubes, or fibers (Fig. 5a).

For CNSs with a low electric conductivity allowing the penetration of an electric field into a volume, the field can also be locally enhanced by the internal-structure elements (Fig. 5b). This results in the formation of conducting channels in the CNS [18, 28, 67, 90–93] which, like conducting external spikes, can concentrate an external electric field. In the case of polycrystalline diamond films, conducting

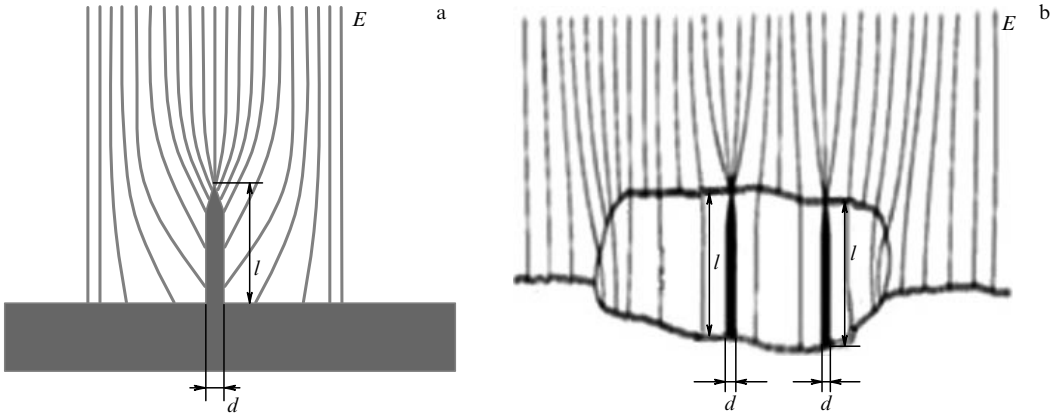

Figure 5. Qualitative picture of the concentration of field E near the external (a) and internal (b) elements of a CNS with the ratio of the length (height) l to width d equal to β.

channels are often assigned to grain boundaries where sp^2 carbon is present in a considerable amount [92, 94, 95].

To confirm this hypothesis, the emission characteristics of a diamond-like film were studied in [18] at various cathode–anode distances. The dependence on the distance obtained proved to be the same as that for emission from CNTs [96] and point cathodes [97]. Since the topography of surface samples studied in [18] did not contain spikes, we can conclude that conducting structures similar to nanotubes in their properties were formed inside the film.

A simple theoretical description of the concentration of the applied electric field by individual parts of the cathode surface can be obtained from the FN theory by replacing the average field strength E between the cathode and anode by its 'geometric-concentration' enhanced value βE. The field enhancement factor β for any particular case is determined by numerical simulations. At the same time, it is known that this factor for a single cusp with height l and radius r of the cusp end for $l \gg r$ is given by a simple expression,

$$\beta \approx \frac{l}{r} . \tag{12}$$

The main change concerns the barrier shape, determined now by the higher field strength $\beta E \gg E$. As a result, the barrier width decreases and the tunnel current through the barrier considerably increases. The current is still determined by the FN law (see (1) and (6)), but with a reduced work function of the emission center:

$$\varphi_c = \frac{\varphi}{\beta^{2/3}} . \tag{13}$$

3.1.2 Drawbacks of the concentration model. The field concentration model is long known and is widespread [98].

However, to explain efficient work functions of the order of a few tenths or even hundredths of an electron-volt inherent in the field emission from CNS cathodes, the relation $300 < l/d < 8000$ should be fulfilled. Such a ratio of the cusp length to its width cannot be inherent in the film surface. Even for CNTs, as shown in [60, 99], the β factor calculated from (12) is 2–4 times larger than the l/d ratio. This drawback is absent in the 'ladder model' (see Section 4.1.1).

Despite the increased resistance of CNTs to the action of destruction factors, it is these factors that remain one of the main reasons restricting practical applications of CNT cathodes [100–102]. Most often, the emitting region of a nanotube and the nanotube–substrate [103] (or matrix) [104] contact region are destroyed. The ion [101, 105], mechanical [103, 106], and thermal [101, 107–109] destructions are assumed to be the main factors producing CNT degradation and vacuum-gap breakdown.

One of the actively studied ways to increase the stability of an emitting region is to exploit the 'blade' geometry using graphene layers with a free boundary oriented in the direction of the acting field (see, e.g., [110–112]). In this case, by decreasing β somewhat, an increase in the thermal and electric conductivity and the mechanical stability of the emitting structure is achieved. Such structures are known under various names: nanosheets [113, 114], nanowalls [115, 116], multilayer graphene [113, 117], and others [35, 36, 118–120].

Despite all the advantages, the application of the enhanced-field model to CNS cathodes is usually complicated. The main reason is the considerable discrepancy between experimental data and emission characteristics predicted by the model, such as the threshold field and the slope of current curves in the FN coordinates (see Fig. 2). The emission characteristics of DLC films for measured work functions φ of carbon gave the estimate $\beta \geqslant 5000$ [25, 37]. At the same time, the geometrical size of carbon fibers located on the surface corresponded to $\beta \sim 50$ [37]. A similar discrepancy was observed in other experiments, where microscopic images of the CNS surface exhibited sharp cusps [26, 99].

Similar complications in the application of the model with the β factor exist for CNSs with an assumed field enhancement by inner-structure elements (see Fig. 5). Calculations in [90, 121] show that, as in the case of an individual elongated element of the external structure, if a structural element with length l formed inside a DLC film has a width $2r$ of the uncharged sp^2 part on the surface facing the anode, the electric field will be amplified $\beta = kl/r$ times ($k = 0.5-1.0$).

The field can also be amplified in internal gaps, e.g., between an sp^2 cluster and a substrate. Here, the β factor is estimated as $\sim l/h$, where h is the gap width [67, 121]. For nonspherical, elongated inclusions, this factor can reach several hundred [93, 121]. However, even this is insufficient for explaining experimental emission spectra [14, 22, 33, 35]; an explanation would require assuming [33] that a nonconducting film contains conducting channels about 10 μm in length with a spike radius of the order of the atomic radius.

Obviously, such an assumption is incorrect, at least for submicron emitting coatings.

The β factor model does not explain the double hump energy distributions of emitted electrons (see Fig. 4) or the hysteresis and correlations of local fields from different regions of the emitter described in Section 2.4. Aside from this (see [122]), the assumption about electron tunneling in diamond-like films from the valence band in the amplified field does not agree with the observed strong dependence of emission properties on the degree of donor impurity doping.

Because of these discrepancies with experimental data, pointing out the contribution of the field amplification by the elements of the surface or volume of carbon films to the decrease in the emission threshold, we should nevertheless note that such an amplification cannot be the only reason for emission. The nature of additional or alternative emission-activation mechanisms is explained by various hypotheses discussed in the next sections.

3.2 Electron emission from a diamond-like film

3.2.1 Description of a two-barrier model. The concentration model focuses all attention on how a barrier between a film and vacuum is overcome. In a two-barrier model [123] (Fig. 6), the emission process involves overcoming two barriers: the first from a substrate to the conduction band of the film, and then electron drifts to the surface and escapes to the vacuum through/over the second barrier. The main focus is devoted to the first barrier between the substrate and film.

The model assumes that a CNS film is a dielectric (diamond-like film!). Obviously, an external applied field penetrates into such a film. The film lies on a conducting (metal) substrate, and when a voltage is applied to it, the film is in a state close to breakdown, i.e., a state corresponding to the exponential dependence of the current of voltage. Such a state is often called the 'prebreakdown' state. A model ignoring the influence of a barrier between the film surface and vacuum on emission processes (see, e.g., monographs [3, 124] and review [125]), called the 'prebreakdown' model or the film–substrate model, can be considered outdated at present.

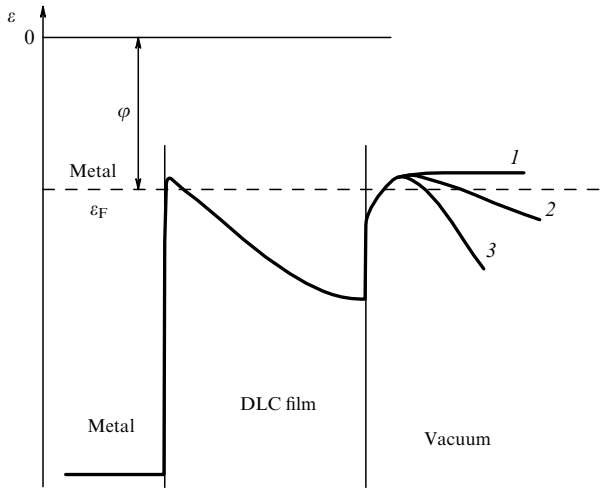

Figure 6. Two-barrier model. The first barrier is located between the conducting (metal) substrate and DLC film. The second barrier is located between the DLC film and vacuum. Lines *1*, *2*, and *3* correspond to different external fields (increasing with the number). Other notation as in Fig. 1.

In the considered two-barrier model of emission from CNSs, emission occurs with the participation of 'hot' electrons overcoming the potential barrier near the surface due to the energy they obtain from the electric field inside the emitter.

The two-barrier model for donor-impurity-doped DLC films on metal substrates is described in papers [122, 126–128]. Because of the great difference between the work functions of a metal and diamond-like regions, a transition layer depleted with mobile carriers is formed near the boundary where impurity atoms are ionized due to the escape of electrons to the metal. The transition layer width is small, while the electric field strength produced by the ionized impurity is high. In combination, this makes possible a tunnel transition through the potential barrier at the substrate–film boundary for electrons from the metal Fermi level. This is the first barrier.

The applied additional external field produces a potential drop also mainly in the depleted transition layer [12]. This is the second barrier.

The emission current in this model is mainly limited by electron injection through the substrate–CNS boundary and should be determined to a greater degree by the properties of this boundary than by the properties of the CNS surface. This conclusion is supported by experimental data: the increase in the substrate roughness caused by mechanical or chemical processing before the deposition of carbon films considerably improves the emission ability [128–130].

The two-barrier model can be modified for DLC films on semiconductor silicon substrates with hole conductivity [131]. The emission current for this material is determined by the spatial charge of holes accumulated in the substrate (see [126] and references therein).

The inelastic scattering of conduction electrons in dielectric films also explains some other experimental facts, in particular, the nonmonotonic dependence of the emission current on the coating thickness [16, 90, 132, 133]. According to calculations, the best emission ability of the covering can be achieved at a certain thickness.

At the same time, in [89] 'two-hump' FEEDs for films consisting of nanographite regions are explained by the two-barrier model despite the absence of carbon in the diamond-like state in their composition.

3.2.2 Drawbacks of the two-barrier model. Despite the fundamental simplicity and acknowledged applicability of the two-barrier model, a number of questions related to the model remain unsolved, at least for some materials and structures.

The main disadvantage of the model is the unclear nature of processes on the substrate–film boundary. For electrons to pass easily thorough a dielectric film, the film should be in the prebreakdown state. However, by considering the prebreakdown state (see, e.g., monographs [3] and [126]), it is always unclear how to keep the boundary between the breakdown (during the breakdown, all is clear (!)) and the prebreakdown state. Note that such a prebreakdown state should be assumed stationary: in experiments, emission is observed for several days or months [85].

A known objection (see Section 4.2 below) concerning the two-barrier model is related to the assumed absence in it of the screening of an external field by a surface charge. However, the penetration of the external field into the film should cause a shift of the local Fermi level and the charging

of surface states. In addition, the energy loss by some of the electrons injected into the film should lead to their accumulation near the bottom of the conduction band in the near-surface region, because the external field strength of about several V μm^{-1} is insufficient to provide their emission into the vacuum from such states. The charge of these electrons should also screen the substrate–film interface from the external field action and stop the injection of hot carriers into the film. Reasons that could prevent the accumulation of a surface charge remain unclear for the range of applied field strengths under study.

3.3 Influence of fields related to emitter inhomogeneity

3.3.1 Description of the 'patch fields' model. Contact phenomena, e.g., the redistribution of charges in laterally inhomogeneous (inhomogeneous along the surface) CNSs produce electric fields in vacuum near the surface, which are sometimes called patch fields — the fields related to electronic structures near the surface of one or another nanosize region.

The patch fields model is based on an estimate of the influence of the surface inhomogeneity (lateral inhomogeneity) on the emission current. This model is described best of all in [48, 134, 135]. For example, the processing of the surface by hydrogen increases the difference between surface properties (contrast) of regions containing sp^2 or sp^3 hybridized carbon atoms. In regions with a dominating sp^2 phase of carbon, the closure of free bonds — the hydrogen termination — does not occur. It is assumed that surface regions with a characteristic size of about 10 nm without hydrogen termination play the role of ECs in planar DLC films producing the local concentration of the applied field [134].

An estimate of the strength of local electric fields related to the electron filling of the surface states of diamond crystallites in efficiently emitting nanocomposite diamond-graphite films gives values of $10^7 - 10^8$ V cm^{-1}, sufficient for a considerable enhancement of the local field of microcusps and the field concentration corresponding to such a geometry.

The obvious advantage of the patch fields model is that it naturally describes the correlation of the better emission properties of CNSs with their well-known inhomogeneity on the nanometer scale (see Section 2.2).

The model also explains the decrease in the effective work function compared to that of graphite-like carbon, albeit, only by 1–2 eV.

3.3.2 Drawbacks of the patch fields model. The inhomogeneities of the emitter surface determine complex energy distributions of emitted electrons. However, patch fields models in their usual form [12, 134] can be applied only for a particular material. As a rule, they do not assume a deviation of the FEED from (8) (see, however, [14]).

As a whole, we should admit that the consideration of lateral inhomogeneity of the CNS surface offers additional possibilities for explaining experimental facts only in combination with many of the emission models discussed here. The patch fields model is a useful idea rather than a particular model for CNSs. Because of this, the agreement between the patch fields model and experimental facts presented in Section 2 is difficult to estimate.

3.4 Dimensional effects: surface levels and resonance tunneling

3.4.1 Description of the surface level model. The model is based on the assumption [11, 13] that the boundary layer of a cathode containing CNSs changes under conditions required for the appearance of emission. In this layer, special regions appear — quantum wells (Fig. 7) with the energy spectrum described by the relation

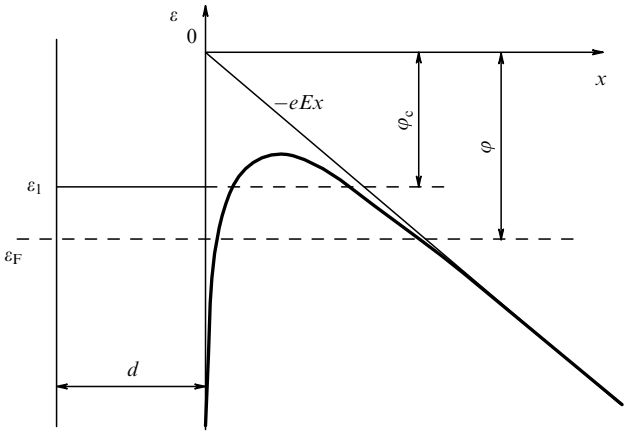

Figure 7. Typical energy diagram of the model of surface levels. The figure differs from Fig. 1 in that the cathode material has a quantum well of width d near the surface. The energy of the first level in the quantum well is ε_1. The effective work function of electrons from this level is φ_c.

$$\varepsilon_k = \frac{\pi^2 h^2}{2md^2} k^2, \qquad k = 1, 2, \ldots . \tag{14}$$

For small sizes d of appearing regions, the effective work function $\varphi_c \approx \varphi - \varepsilon_k$ becomes small.

Obviously, small effective work functions correspond to $\varepsilon_1 \approx \varphi \approx 4$ eV. This energy corresponds to the EC size $d_c \approx 1.5-2$ nm. This value is somewhat smaller than the usually accepted EC size ($\approx 4-5$ nm). Thus, the surface level model well explains small values of the work function.

3.4.2 Drawbacks of the surface level model. It is assumed in [11] that surface levels are produced due to the formation of a thin layer of sp^2 hybridized atoms on the body of sp^3 hybridized atoms. However, such layers have not been found.

Attempts to observe surface layers by the methods of cathodoluminescence [25] or Auger spectroscopy [13] were unsuccessful in the opinion of the authors of these papers themselves. Attempts to treat surface levels as manifestations of quantum dots [14, 136] were also unsatisfactory. The objects of all these studies had sizes of more than 5–10 nm, which is almost an order of magnitude larger than the size required by the model.

Note that this model can probably be applied only in combination with the concentration model. Otherwise, to explain the low values of the work function φ_c determined from FN emission characteristics, it would be necessary to assume the existence of the normally filled emitter states with energies ε_1 different from the vacuum level only by φ_c, i.e., by fractions of electron-volts. Obviously, at room temperature this would be accompanied by thermionic emission that was not observed in experiments.

Calculations [14, 33] show that, for a thickness of the graphite shell of diamond grains on the order of 1–2 graphene layers, the surface barrier height (the effective work function φ_c) for the shell decreases to approximately 1 eV. Taking into account the additional concentration (geometrical) enhance-

ment of the field by the graphite shell, the 'compromise' value φ_c explains both the presence of low-voltage emission and the absence of thermionic emission at room temperature. This estimate agrees well with the effective work function estimated in experiments with a tunnel microscope for graphite-like cusps with different heights d [137]. For $d \approx 3$ nm, the work function decreases by half compared to the bulk material.

Note that an alternative emission mechanism in [14] may be electron transfer to the vacuum through the surface states of diamond crystallites, which can also be considered the limiting case of a reduced-dimension system.

These model results agree well with experimental papers [46, 58, 92, 138, 139], where the best emission properties of CNS materials were obtained namely for structural inhomogeneities close to 1 nm in size. At the same time, other publications [10, 16, 42–45, 48, 71, 74, 140, 141] report that the maximum emission ability is achieved at considerably larger CNS sizes of the order of 10 nm or even several dozen nanometers. In this case, the quantum-dimensional decrease in the work function might not be considerable. Thus, the explanation for the emission ability of CNSs by the properties of reduced-dimension structures is not universal, i.e., is not valid for all CNSs.

The surface level model does not explain the two-hump FEED (see Section 2.5). In the simplest case, this model predicts the FEED in the form of the only narrow peak. More exact calculations in [113, 142] show, however, that this peak can have a rather complicated structure. Taking into account that the cathode surface can be nonequipotential [31] and the possibility of the existence of numerous emission centers, this peak can be broadened, but it is unlikely that its splitting and the transformation of its shape upon changing the applied field can be expected [89].

However, the most convincing objection against the correctness of the surface level model seems to be the following: surface regions with the work function much smaller than that of the environment, even with a small area, should also be detected by measuring the work function by alternative methods not related to the field emission. As mentioned in Section 2.3, such measurements were performed for CNS emitters many times [10, 26, 44, 45, 66, 67, 143], but regions with a low work function were not found.

Such essential disadvantages of the surface level model make useless attempts to explain other features of field emission from CNSs considered in Section 2 within the framework of this model.

Note that surface levels can play some role during the transition process of the emission current growth after the external field is switched on, but under stationary conditions, their influence can be disregarded.

3.4.3 Resonance tunneling: the development of the surface level model. Many of the difficulties of the surface state model are successfully avoided in the model of emission due to resonance tunneling through a double surface potential barrier. This model also uses a hypothesis about the existence of surface levels. It differs from the surface level model in that the emitting electronic states of surface structures with discrete energy levels in the absence of the field are assumed to be unfilled. Because of this, they are not found during the measurement of the work function in the absence of the field or in a weak field. In a stronger electric field, the energy of such states decreases due to penetration of the field to the emitter (Fig. 8). When this energy decreases to the energy of the filled bulk states, the process typical of a two-barrier model considered in Section 3.2.1 becomes possible. The authors of [144] discussed variants of the complete, partial, or absence of coherence of the waves reflected from two barriers during the electron transfer from the volume to vacuum. The discrete levels of surface structures play the role of the first barrier which under some conditions [144] makes emission more efficient than in the case of a direct transition from the surface to vacuum according to the FN mechanism (second barrier).

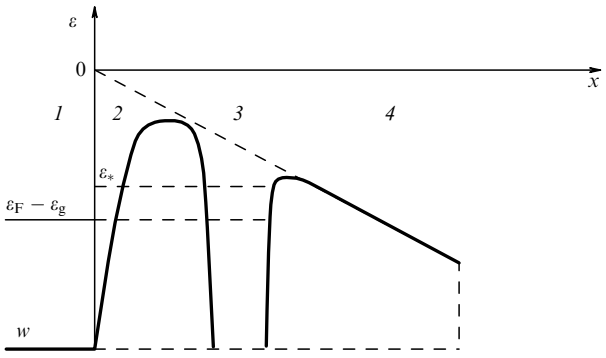

Figure 8. Characteristic energy level diagram of the resonance tunneling model in the coherent case. It differs from the diagram in Fig. 1 in that the barrier is divided into two parts (*2* and *4*) by quantum well *3* with the energy level ε_*. The relative height and width, as well as the relative position, of barriers *2* and *4* with respect to each other are not important for qualitative conclusions. Cathode *1* can be either a metal (with the Fermi energy ε_F), or a semiconductor (with energy ε_g of the conduction band bottom). w is either the bottom energy of the filled band or the valence band boundary.

In the region between these barriers, a level with energy ε_* is located, which can be estimated from (14). The solution of the Schrödinger equation for this system is rather complicated (see, e.g., [13] and references therein). It was found that for some value ε_* resonance tunneling appears. This means that the transparency of two barriers in this system is higher than that of each of the barriers separately.

The calculation of the current density for resonance tunneling is formally performed in the absolutely same way as the calculation leading to the FN law (see Eqns (4) and (5)). Of course, in this case, the potential shown in Fig. 1 is replaced by the potential corresponding to that shown in Fig. 8. Constants A and B are not specified by relations (2), but are transformed to some functions. The constant A is transformed into $A(y)$ and B to $B(y)$. The dimensionless parameter y is written (recall that ε_0 is the permittivity)

$$y = \frac{e^3 E}{4\pi\varepsilon_0 \varphi^2}\,. \tag{15}$$

Functions $A(y)$ and $B(y)$ are written in the form of polynomials (see, e.g., [145] or [136]). The transparency corresponds to $B(y) = 0$. In a very rough approximation, this leads to $y \approx 1$ and the corresponding energy level

$$\varepsilon_* = \varphi - \sqrt{\frac{e^3 E}{4\pi\varepsilon_0}}. \tag{16}$$

In Ref. [145], resonance tunneling is considered near the substrate–film interface and helps to refine the prebreakdown

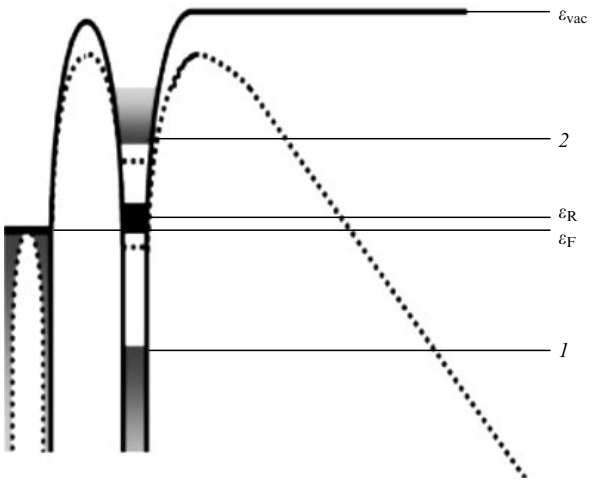

Figure 9. Another energy level diagram of the resonance tunneling model in fields. It differs from Fig. 8 in that the barrier is divided by a quantum well with two allowed bands (*1* and *2*). The position of resonance levels (ε_R) in the Fermi level region is shown in the 'incoherent case'. The solid curve corresponds to the absence of an external field, and the dotted line corresponds to the applied field (see Fig. 1). (Taken from [38].)

model, applying it to semiconductor substrates. In [136], it is assumed that resonance tunneling occurs near the boundary of the main collection of sp^3 hybridized atoms and a thin layer of sp^2 hybridized atoms covering the collection.

Resonance tunneling can occur in different ways in the emission process (see, e.g., Fig. 9).

Volt-ampere characteristics for such a material consist of series of steps whose positions depend on temperature and the 'direction' of a change to the applied voltage. They are characterized by a strong hysteresis. The hysteresis is explained by the accumulation of a charge in a quantum well in which the positions of levels also depend on temperature. Such structures can be used in memory devices.

The resonance tunneling model may be proposed to describe the features of low-threshold emission from diamond microcusps in fields of ~ 10 V μm^{-1} [76]. Based on the results of analysis of the current, FEEDs, and volt-ampere characteristics, we can conclude that the most efficient emission mechanism is resonance electron tunneling from microcusps through the states of individual molecules adsorbed on their surface.

3.4.4 Drawbacks of the resonance tunneling model. It is obvious in the case of coherent resonance tunneling that the total reflection coefficient will strongly decrease only when the amplitudes of reflected waves for both barriers are close to each other. For different shapes of the surface and usual barriers, this condition can be fulfilled only in a narrow range of the applied field strengths. The simultaneous fulfillment of several resonance conditions (the closeness of the amplitudes of reflected waves, their opposite phases, and the closeness of the resonance level to the Fermi level of the volume) seems unlikely at the same field strength.

Calculations based on the resonance tunneling model are more justified than those based on the surface level model (see Section 3.4.1). Thus, it is assumed in [145] that the barrier is separated into two because of the presence of positively charged impurities near the silicon substrate–film interface in CNSs. This assumption was made earlier (see [3, Ch. 25]) to explain the properties of the prebreakdown state. However, calculations of this type are similar to engineering calculations.

The obvious advantage of the resonance tunneling model is the opportunity to explain the hysteresis and complicated form of volt-ampere characteristics. At the same time, concerning the possibility of applying this model to emission from CNSs, one should take into account that the model assumes the necessity of a considerable (comparable to the work function) shift of the working level of a quantum well near the surface of a carbon structure. This shift occurs due to a decrease in the barrier height at the boundary with the vacuum, which already has a sufficient tunneling transparency, i.e., has a width smaller than or around 10 nm. Therefore, considerable additional local field strengths are required from several hundred to thousands of V μm^{-1}. However, such field strengths can be quite easily achieved upon additional field enhancement. For diamond microcusps (see [76]), the reason for such enhancement is obviously the β factor. In the case of a DLC film [21], the field was probably enhanced by the β factor of the internal structure elements (see Fig. 5). At the same time, in the absence of the possibility of field enhancement, it is unlikely that resonance tunneling can be observed at field strengths below 100 V μm^{-1}.

4. New models of field emission from materials with carbon nanostructures

4.1 Porous materials: ladder model

4.1.1 Description of a ladder model. To explain the emission of electrons at low applied voltages from 'porous' carbon materials, a model combining the elements of the β factor model and the influence of quantum-dimensional effects is proposed [146]. Materials are called porous if their surface always contains graphene scales or flakes. In an external electric field, a kind of 'ladders' of benzene rings (structural elements of graphene sheets) (Fig. 10a, b) can stretch from the

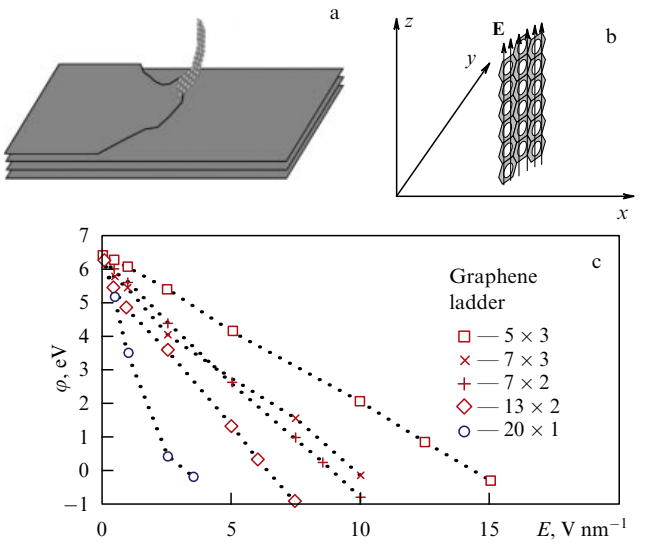

Figure 10. (a) Graphene ladders on the surface of porous carbon materials; (b) model of a graphene ladder consisting of 6×3 benzene rings; (c) dependences of the surface barrier height (the effective work function φ of electrons) on the applied external field E for ladders of various sizes.

surface of such a CNS along force lines. Because interplane bonds in non-single-layer graphene are, of course, considerably weaker than bonds acting in a graphene plane themselves, electric forces can be sufficient to lift 'ladders,' but insufficient for their complete detachment from the surface. The numerical estimate made in [146] shows that, to support the structure shown in Fig. 10a in the vertical position, it is sufficient to transfer to it only one redundant electron, whereas, to detach the structure completely, it should contain no fewer than 10^3 redundant electrons.

Obviously, a graphene ladder can concentrate an electric field, which allows one to assign to each such structure a β factor considerably exceeding unity, especially if the ladder length is considerably (tens of times) greater than its transverse size. However, according to estimates in [146], the values of β for expected ladder sizes remain insufficient for explaining the results of many experimental studies. Therefore, it was also proposed to take into account a decrease in the potential barrier height corresponding to a decrease in the effective work function caused by the partial penetration of the applied field into the ladder material. This effect significantly differs from the Schottky effect ([3, Ch. 12] and Fig. 1), which gives a decrease in the work function proportional to the square root of the field strength. In the case considered here, the height of a surface barrier (the effective work function) for an atom at the ladder end linearly decreases upon increasing the applied field, and the faster it does so, the higher the ratio of the longitudinal and transverse sizes of the carbon structure. The results of simulations [146] presented in Fig. 10c show that this decrease can be rather significant even for relatively short ladders, e.g., consisting of 20 benzene rings: from 6.0–6.5 eV in the absence of the field down to values close to zero at field strengths of about several thousand V μm^{-1}.

Note that a problem similar to that in [146] was also solved for nanotubes, e.g., in [147, 148]. Because of the large cross section of nanotubes, even single-wall ones, the degree of penetration of the electric field obtained in these calculations proves to be smaller than that for the case of ladders in [146]. The main advantage of the graphene ladder model is that it can explain the main experimental facts concerning emission from heterogeneous (porous) nanocarbon materials. The absence of direct experimental evidence of the existence of ladders is related to the complexity of their detection.

4.1.2 Drawbacks of the ladder model. Note at the same time that, according to calculations [146], the macroscopic field strength required to obtain a high enough emission current is, however, rather high, reaching at least hundreds of V μm^{-1}, whereas emission has been observed in many experiments in much weaker fields. In addition, a simple summation of field enhancement effects on the sharp end of a ladder because of its concentration and the decrease in the surface barrier caused by the field penetration into the ladder structure does not seem completely correct, because the field penetration reduces the β factor [148, 149].

Another disadvantage of the model discussed here is that it paradoxically does not explain the low values of the effective work function determined from FN experimental characteristics. According to (6) and (7),

$$\ln\left(\frac{j}{E^2}\right) = f\left(\frac{1}{E}\right) = \text{const} + B\,\frac{\varphi^{3/2}}{E}\,. \tag{17}$$

The slope of the characteristic is $B\varphi^{3/2}$. We assume for simplicity that the effective work function (the surface barrier height) decreases with increasing field as

$$\varphi^{3/2} = \varphi^{3/2}(0) - \alpha E\,, \tag{18}$$

where $\varphi(0)$ is the real work function equal to the surface barrier height in the zero field. By substituting (18) into (17), we obtain

$$\ln\left(\frac{j}{E^2}\right) = f\left(\frac{1}{E}\right) = \text{const} - \alpha + B\,\frac{\varphi^{3/2}(0)}{E}\,. \tag{19}$$

Thus, the consideration of the field decrease in the surface barrier in form (18) does not change the slope of the FN characteristic, but only causes its parallel displacement. When a linear decrease in the barrier height with the field is specified by formula (18), which corresponds to most calculated plots in Fig. 10c, the consideration of the field effect somewhat changes the slope and shape of the FN characteristic, but obviously not very strongly.

4.2 Influence of the interelectrode space: optimal vacuum model

4.2.1 Description of the optimal vacuum model. Model [150] assumed that the layer of a positive charge is formed at the film–vacuum interface. The emitting element of a CNS is a thin dielectric layer on a conducting part of the film surface. The surface of this layer acquires a positive charge. The charge is produced due to the deposition of positive ions here generated in a vacuum gap by ionizing a residual gas by emitted and accelerated electrons (see [3, Ch. 26] and references therein). Ions are neutralized on conducting surfaces; however, they can be accumulated in the presence of diamond-like-phase regions. Such regions form a virtual positively charged 'network' located in front of the substrate and playing the role of a 'real' cathode in a vacuum triode.

It is easy to show that the field strength produced by an ion charge with the average density σ is described as

$$E = \frac{e\sigma}{\varepsilon\varepsilon_0}\,. \tag{20}$$

This field is added to an external electric field and can considerably (by orders of magnitude!) exceed it. In this case, the role of the external field is mainly determined by processes in the vacuum gap.

Estimates show that, to extract electrons into a vacuum, the surface ion density should be $\sigma = 10^{13}$ cm^{-2}, corresponding to a mean distance between ions of ~ 4 nm. The gas pressure corresponding to the equilibrium between the arrival rate of ions on the surface and their neutralization rate for this ion charge density proves to be 10^{-5} Pa, which agrees with conditions of many emission experiments.

The advantage of this model is that, aside from emission itself in a relatively weak external field, the model also explains the hysteresis of emission properties determined by the accumulation of a surface ion charge. The presence of a broad low-energy peak in the energy distribution of emitted electrons (see Fig. 4) in the optimal vacuum model is explained by inelastic scattering in an sp^3 layer. However, in this layer, this scattering can be insignificant, and then the FEED should contain the only peak with the energy of the emitting states of the substrate, which also corresponds to experimental data.

Note that a layer of positive ions is not formed on the surface of metal cathodes [150].

4.2.2 Drawbacks of the optimal vacuum model. The optimal vacuum model is an alternative in some sense to the field concentration model (β factor model). The β factor model can explain the small values of the effective work function, but cannot explain all the other features of field emission from CNSs. In the optimal vacuum model, it is the small effective work functions that are most difficult to explain. Thus, the effective work function for emission from diamond-like films [11, 13, 123, 151–156] changes by at least an order of magnitude, whereas the model predicts in fact the same values. However, many other features of field emission from diamond-like films are explained, although not without issues, by this model.

The optimal vacuum model, which would be better to call the film–vacuum model [150], explains well the properties of field emission from CNS films. However, the mechanism (process!) of formation of too great a number (10^{22} m^{-2}) of positive ions on the surface of a diamond-like film remains unclear.

Finally, this model is absolutely invalid for conducting CNS materials.

4.3 Influence of a thermoelectric field on emission from carbon nanostructures

4.3.1 Description of a thermoelectric model. The model of electron emission from CNSs assumes the existence of an anomalously strong thermoelectric effect in CNSs [157–159]. The thermoelectric effect is initiated by the heat release in ECs. According to the model, an EC is a graphite-like nanometer region surrounded by regions containing sp^3 hybridized carbon (Fig. 11). The emission current is a thermal source determining the EC temperature (T_h) different from the temperature of surrounding diamond-like regions (T_c).

The heat flow in the sp^2 carbon is determined by the phonon propagation — the phonon wind [158]. The phonon flow transfers charge carriers (electrons) into an EC and produces the thermal electromotive force $\gamma\Delta T \equiv (\alpha k_B/e)\Delta T$ in it. Here, γ and α are the usual and dimensionless thermoelectric coefficients, and $\Delta T = T_h - T_c$. The thermoelectric field distorts the energy structure of ECs (Fig. 12) compared to the structure adopted in the FN law (see Fig. 1) by increasing the energy of part of the electron gas by the value of the thermal e.m.f. The surface barrier height for such electrons proves to be reduced (φ_c in Fig. 12), which can facilitate emission.

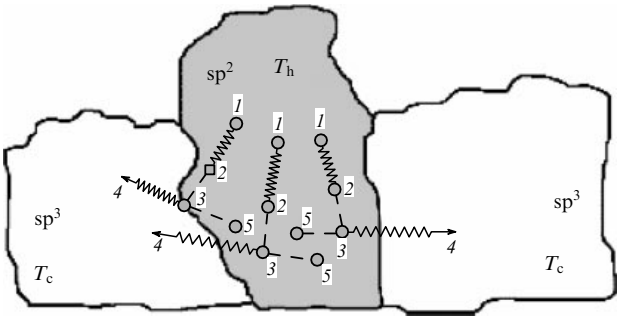

Figure 11. Thermoelectric effect in an EC in carbon nanostructures. In a graphite-like region (sp^2) having the higher temperature T_h (because of energy losses during emission), electrons (*1*) absorb phonons (*2*) and are dragged by phonons in the phonon-wind (thermal flow) direction. Their relaxation (*3*) occurs with phonon emission in a random direction. Emitted phonons escape from the EC, coming to diamond-like (sp^3) regions (*4*) with a lower temperature T_c, which play the role of a cooler, while electrons remain in the sp^2 region (*5*).

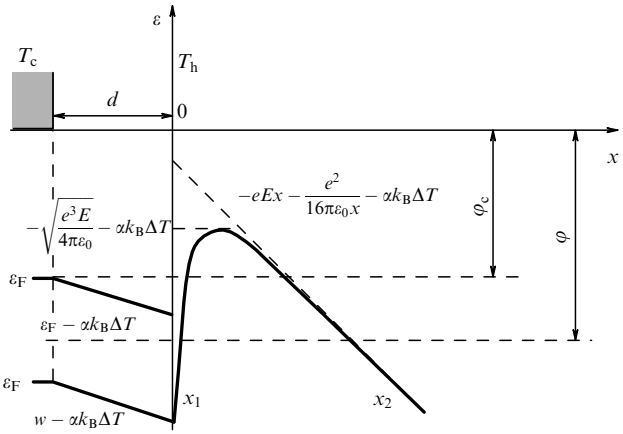

Figure 12. Energy level diagram for the thermoelectric model. The electric field produced due to the thermoelectric effect because of the temperature difference $\Delta T = T_h - T_c$ (see Fig. 11) in an EC characterized by the dimensionless thermoelectric coefficient α determines the slope of band boundaries. As a result, the work function φ decreases by $\alpha k_B\Delta T$ and becomes equal to φ_c.

A special feature of CNSs [157–166] is the unique character of the interaction of phonons with charge carriers providing anomalously high values of the thermoelectric coefficient. Because of the small size of ECs, phonons in them barely collide with each other and are not thermalized. Therefore, for $T_h \gg T_c$ and weak reflection of phonons from the boundaries of ECs with sp^3 regions, the phonon flow is unidirectional and ballistic, and the main mechanism of its action on charge carriers even at high temperatures is the ballistic drag of electrons by ions.

The work function is described by the expression

$$\varphi_c = \varphi - \alpha k_B \Delta T . \qquad (21)$$

A more accurate calculation of the emission dependence gives the expression coinciding with FN (1), where the constant B is replaced by the quantity

$$B_T = B\,\frac{1}{\varphi^{3/2}}\left[\varphi^{3/2} - \frac{3}{2}\,\alpha k_B\Delta T\left(\varphi - \frac{1}{2}\,\alpha k_B\Delta T\right)^{1/2}\right]. \qquad (22)$$

It is easy to show that emission dependences based on Eqns (21), (22) and (1), (2) differ only in the third order of smallness in ΔT.

For $\alpha = 100$ [162], expression (21) predicts a decrease in φ_c to zero already for $\Delta T \approx 400$ K. Such temperature values seem quite plausible [32]. It is known that in the case of a high current, ECs in CNSs can emit radiation with the 'thermal' spectrum corresponding to temperatures of about 1000 °C. In addition, the EC temperature estimates in [82] from the FEED spectra [83] discussed in Section 2.5 gave values about 2000 K.

Aside from the broad width of energy distributions of emitted electrons, the thermoelectric model also explains their splitting into two components (see Fig. 4). The presence of electrons with energies near the Fermi level of the substrate or

cathode volume is explained by the possibility of their escape into the vacuum through thin sp^3 layers according to the two-barrier mechanism considered in Section 3.2.

In fact, the thermoelectric model discussed here explains the emission of electrons with a low threshold voltage by the production of thermoelectric fields acting on the emission process, similarly to the action of patch fields (see Section 3.3.1) in models considered earlier. For this action to be significant, the thermoelectric field strength should approximately correspond to the local external field strength required for emission in the FN model, i.e., should be of the order of 10^9 V m^{-1}. According to estimates [157–159], such a thermoelectric field strength can be achieved in the structure under study due to the features of the thermoelectric effect in them.

Taking into account the assumptions made above, the thermoelectric model proposed here well describes many features of emission from CNSs, in particular, the possibility of emission itself from CNSs at low applied voltages with cathodes without distinct cusps, the small slope of emission dependences in the FN coordinates, and the FEED shape.

4.3.2 Drawbacks of the thermoelectric model. At the same time, the model has some obvious disadvantages. Although the heating of ECs up to temperatures on the order of hundreds or even thousands of degrees seems possible, the capability of producing such a large temperature difference ΔT inside a graphite region is doubtful.

Let us make a quantitative estimate for an EC $d = 10$ nm in size, where the thermal power $P = 1$ μW is released, which corresponds to a current of 1 μm and the release of 1 eV of energy in an EC by each emitted electron, the latter energy being most likely considerably overestimated. The thermal flow density in the EC is estimated as $q \sim P/d^2 = 10^{10}$ W m^{-2} $= 1$ MW cm^{-2} (!). The heat conduction of graphite strongly depends on various factors. Let us take the typical macroscopic value $\kappa = 100$ W m^{-1} K^{-1}, which is, of course, unacceptable. Despite a rather high thermal flow density, the temperature drop over the EC size proves to be small: $\Delta T \sim qd/\kappa = 1$ K. This corresponds to the general rule pointed out, for example, in [165], according to which temperature drops in nanostructured media with the lattice heat conduction occur mainly at the region boundaries, because the length of the homogeneous regions of the structures themselves is insufficient for the noticeable absorption of the phonon flow.

The phonon flow is attenuated at the boundaries due to its partial reflection and is characterized by the thermal Kapitsa resistance R_K relating the temperature drop at the boundary with the thermal flow density [166] as

$$\Delta T_b = R_K q\,. \tag{23}$$

The values of R_K for many different pairs of media separated by interfaces lie in a rather narrow range $R_K = (0.6-3.0) \times 10^{-8}$ m^2 K W^{-1} [165, 167, 168]. The data for carbon materials can be found in [162, 163, 169]. For the value of q determined earlier, we obtain $\Delta T_b = 60-300$ K. Thus, for the structure considered here and typical EC parameters, temperature drops of hundreds of degrees can indeed be expected, but these drops will occur not in the volume of the sp^2 region, but at the interface between phases, which is not consistent with the emission mechanism proposed in [157–159].

Another weak point of the thermoelectric model [157, 158] is the difficulty of matching the energy balance of physical processes involved in the model. The source of thermal energy in the model is probably the energy lost in ECs by the same electrons that are later emitted. It seems that even for a 100% thermoelectric transformation efficiency, this energy would be insufficient for imparting to the same electrons the additional energy required to overcome a barrier for emission. At the same time, the nature of possible energy sources is not described in [157, 158].

4.3.3 Islet model: development of the thermoelectric model. The problems mentioned above are taken into account in the islet emission model discussed below, which also uses the concept of increased efficiency of thermoelectric phenomena at the nanoscale.

The islet model is a combined model of emission from a carbon film consisting of separate islet clusters. This model is used to explain the mechanism of low-voltage emission in external fields with strengths from a few hundred V μm^{-1}, which was discovered and studied quite recently [42–45, 71] in carbon films on silicon substrates.

The structural simplicity and small thickness (only a few nanometers) of such films and their availability for detailed studies by surface-sensitive methods make them a convenient object to verify the models of field electron emission alternative to the classical mechanism of tunneling to a vacuum. Experiments have shown that emission is observed only from films containing separate nanosize sp^2 carbon islets without ohmic contacts between them. The film surface does not exhibit any cusps, ladders weakly bound to the surface, or other similar formations. The work function determined by several independent methods is typical for sp^2 carbon. The scatter in the values of the work function determined by emission-independent methods is relatively small: $\varphi = 4.7 \pm 1.0$ eV [44, 45].

Neither of the emission models known so far can explain all the experimental results obtained with these materials (see [44, 45, 71, 170]).

Therefore, we propose a model including the elements of many emission models considered above: the two-barrier model (see Section 3.2.1), patch fields model (see Section 3.3.1), and thermoelectric model (see Section 4.3.1).

According to the islet model [44, 45, 71], an EC includes at least two sp^2 carbon nanocluster islets (Fig. 13a), of which one (A) has an ohmic contact with the substrate, while the other has no contacts with the substrate or other islets. This isolated cluster (islet B in Fig. 13a) acquires a positive charge producing a high positive potential ϕ_{EC}, comparable in value to the work function φ (Fig. 13b):

$$\phi_{EC} \approx \varphi\,. \tag{24}$$

This makes possible the injection of electrons into this cluster from another surface cluster, retaining a potential close to that of the substrate volume (islet A in Fig. 13a).

Because of condition (24), the electron energy proves to be sufficient for emission from islet B of almost all the electrons escaping from islet A to the vacuum, despite the loss of part of their energy — the ohmic heat ($\Delta\varepsilon$) in a charged cluster B (Fig. 13b).

Such losses produce a source forming a phonon flow — a phonon wind — to the substrate (Fig. 13a, wavy lines). According to [32, 82, 170], the difference between the EC

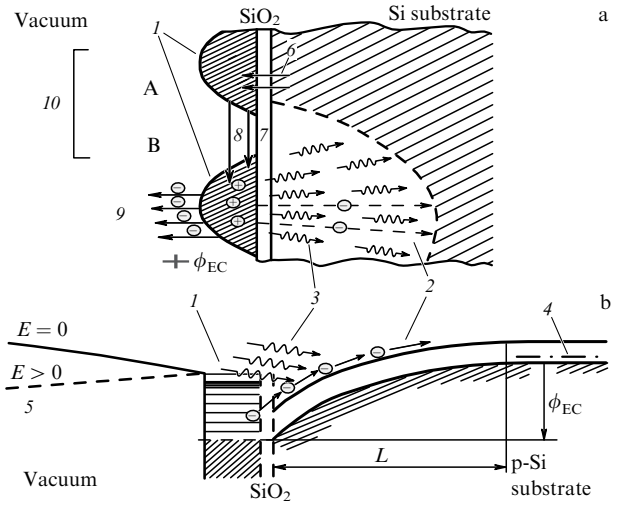

Figure 13. Islet emission model. (a) Diagram of the model, (b) energy level diagram. The sp^2 regions (A and B islets) are denoted by *1*. Near the substrate, positive charges are accumulated in islet B, which appear due to the transfer of electrons to the substrate (*2*) by the heat flow (phonons) (*3*). (b) The Fermi level is shown by *4*. The potential ϕ_{EC} of electrons in islet B weakly differs from the work function. Near the vacuum level (*5*), metastable electronic states in islet A are shown; L is the depth of penetration of an external field into the substrate. Figure a shows the electric current (*6*) from a silicon substrate with the hole conduction (dashes) and islet A (denser dashes) through an SiO_2 oxide layer (*7*). Then electrons tunnel (are injected) (*8*) into islet B, from which electrons are emitted into a vacuum gap (*9*). All this together constitutes the emission center (*10*).

and substrate temperatures for typical experimental situations can be rather large, reaching hundreds and even thousands of degrees Kelvin. The phonon mean free path in crystalline silicone at room temperature (more than 200 nm at 300 K [171, 172]) considerably exceeds the EC size.

The fulfillment of these conditions makes the phonon flow ballistic in the substrate region adjacent to the EC and its action on charge carriers is especially efficient (see Section 4.3.1) [157–164]. Electrons coming to this region of the substrate from its main part or from ECs will be removed from it by the phonon wind oppositely to the action of the EC electrostatic field (Fig. 13b). This results in the formation of a depleted layer in the substrate isolating cluster B, from which, in fact, emission occurs, and in maintaining the positive charge of the cluster.

The author of [71] estimated the cluster size for typical EC parameters as $d = 10$ nm and the heat release power in it as $P = 1$ μW. The thermoelectric field strength estimated as $E_{\text{therm}} \approx 10^8$ V m^{-1} coincides (see [157, 159]) with the estimated EC electric field strength $E \sim \phi_{EC}/L \approx 10^8$ V m^{-1}, where $L \approx 50$ nm is the electric field penetration depth in the substrate (see Fig. 13b). These estimates show that phonons can transport individual electrons from ECs to the substrate against the action of the electric field present in the ECs.

An important feature of the islet model is that the thermoelectric effect in it is the source of additional energy, not for all electrons injected into the emitting cluster, but only for 'lost' (not emitted) electrons, preventing the accumulation of a negative charge. The proportion γ of such electrons in the electron current (from islet A, Fig. 13a) is small, which provides the energy balance conditions. This condition for the model under study is reduced to the requirement for a sufficient amount of thermal power released in the EC to remove all unemitted electrons from it. It is easy to show that this condition can be described by the approximate expression

$$\frac{\Delta\varepsilon}{e\phi_{EC}}\,\eta \geqslant \gamma \quad \text{at} \quad \eta, \gamma \ll 1\,. \tag{25}$$

Here, η is the thermoelectric conversion efficiency, and $\Delta\varepsilon/e\phi_{EC}$ is the mean energy fraction of a hot electron lost by the electron before emission into the vacuum.

To fulfill condition (25), carbon clusters forming ECs should provide the possibility of emitting a greater part of the electrons injected from other islets (e.g., islet A in Fig. 13a), to ensure the smallness of γ, which assumes the presence of metastable electronic states with energies close to the vacuum level (Fig. 13b). In sp^2 carbon islets, they can be states near the bottom of the σ^* band with energy 3.7 eV above the contact point of Dirac cones or the Fermi level of undoped sp^2 carbon. The energy spectrum of a graphite-like nanometer cluster is discretized due to local effects and contains discontinuities of more than $k_B\Theta$ (Θ is the Debye temperature) [81, 170]. This excludes the relaxation of the electron energy with phonon emission in the one-phonon process.

It can be expected that, for electrons with energies above the bottom of the σ^* band of phonon levels, the heat release mechanism remains efficient due to the high density of states in this part of the spectrum and also due to the broadening of levels caused by the finite transparency of the surface barrier (Fig. 13b). As a result, electrons injected into a positively charged carbon cluster (islet B in Fig. 13a) with energy close to $e\varphi$ will rapidly transfer part of their energy to phonons and will be found near the bottom of the σ^* band, from which they can be emitted into the vacuum with small losses.

The model proposed in [44, 45, 71, 170] explains many features of the CNS emission described in Section 2. The emission mechanism in the islet model requires neither the presence of elements providing the field concentration nor a low work function of any regions of the emitter surface — patch fields. The main element of an emission center is an isolated graphite-like carbon nanocluster. Such clusters are present in many types of disordered CNSs.

As in the models of two-barrier emission from DLC films (Section 3.2) and emission in patch fields (Section 3.3), electrons are emitted in the islet model mainly under the action of the electric field of charges located in the emission center. This field is much stronger than the applied external field. Thus, the model explains the small slope of straight lines in the FN coordinates by the small contribution of the external field to the total field acting on a tunneling electron. The islet model also explains the hysteresis of emission from CNSs (Section 2.4) and spatiotemporal correlations of emission currents (Section 2.4 [69–71]). The dependence of emission parameters on the gas pressure [150] is determined by the accumulation dynamics of charges on the emitting surface and by the preservation of these charges for some time after emission termination.

The shape and changes of the FEED (Section 2.5) are also explained. One of the observed maxima (see Fig. 4) may be related to the electron emission from the metastable states of ECs, and the second one, with energy near the Fermi level, to the emission of electrons that did not lose their energy in interactions with phonons in ECs.

Table

Section number	Carbon nanostructures	Models	Properties of field emission from carbon nanostructures								
			1	2	3	4	5	6	7	8	9
3.1.1	Nanotubes; conducting films	Field concentration model (β factor model)	+	–	–	±	+	±	–	–	–
3.2.3	Thick films	Optimal vacuum model	+	+	+	+	–	–	+	+	+
3.4.1	Doped films	Surface level model	+	+	–	–	–	–	–	–	–
3.4.3	Doped films	Resonance tunneling model	+	+	–	–	+	–	+	+	+
4.1.1	Porous materials	Ladder model	+	+	–	±	±	+	–	–	–
4.2.1	Conducting films	Two-barrier model	+	+	+	+	–	+	–	–	+
4.3.1	Thin films	Thermoelectric model		+	+	+	+	+	+	+	–
4.3.3	Thin films on a conducting substrate	Islet model	+	+	+	+	+	+	+	+	+

4.3.4 Drawbacks of the islet model. The substantiated estimate of the combined emission islet model proposed in [44, 45, 71, 170] is hampered by the fact that the model itself is developed only qualitatively at this stage. With the development of a more detailed quantitative theory, either fundamental discrepancies will be found or additional confirmations of its validity will appear. Experimental tests of the model are possible and desirable.

5. Conclusions

Models explaining field emission from CNSs are considered in this review in the order of decreasing degree of applications.

The field concentration model or the β factor model is the most widespread. This model was almost always used to explain the value of the effective work function and, therefore, the observed current. For nanotubes or DLC films with a porous structure, the surface contribution introduced to the emission current by other mechanisms is small and unnoticeable. However, to explain currents from nanotubes decorated with diamonds [60], the β factor alone is no longer sufficient and the field concentration model should be used in combination with the two-barrier model.

The two-barrier model should come in second place by its applications. Like the field concentration model, this model was transferred to the theory of CNS field emission from the theory of field emission from metals. These two models supplement each other well. The mechanism brought about by the field concentration due to the β factor explains the current value, whereas the FEED shape is mainly explained by the energy loss during the propagation of electrons through the film.

However, both models have fundamental drawbacks. From the point of view of the theory, the main disadvantage is that both models refer to possible — but difficult to find — properties of materials from which emission occurs. It would seem that the length/width ratio for nanotubes could be easily determined. However, it is difficult to take into account in calculations the density and randomness of the location of tubes with respect to each other, and this can change the β factor by many times. To find real mounds and dents on a film is even more difficult. As mentioned above, it is unclear in the two-barrier model why the prebreakdown state, which is unstable by definition, exists sufficiently long.

This drawback is absent in the optimal vacuum model, in which a positively charged layer is located at the interface with the vacuum rather than with the substrate. However, this model immediately encounters difficulties with the explanation of the observed FEED shape.

From the point of view of experiments, the main disadvantage of the field concentration and two-barrier models is that they cannot explain or predict the results of measurements of other quantities which could prove that a material indeed has the assumed properties. For example, there are no calculations of light reflection from the surface with a profile giving the required β factor; there are no measurements of the formation and recombination of electron–hole pairs; etc.

The main drawback of models transferred from the theory of field emission from metals is the absence of an explanation of the appearance and operation of ECs. At the same time, the existence of such EC CNSs first assumed in [157] is generally accepted at present.

Other models considered were proposed specially to explain the emission properties of materials with CNSs.

As mentioned above, the independent discovery of many properties, which undoubtedly should be manifested by surface levels, is absent. The mechanism of maintaining the required temperature difference in the thermoelectric model remains unclear, which makes dubious the use of this model as well.

Recently, the tendency has appeared to explain experimental data by combinations of models. Fundamentally, it is unlikely that such an approach is promising, because disadvantages of each of the models do not disappear in this case.

At the same time, CNS cathodes have a number of drawbacks hampering their practical application. They are the inhomogeneity of the EC distribution on the emitter surface, the low average current density, the insufficient stability, and the service time not being long enough. Attempts to increase the total cathode current by increasing the cathode area proved to be inefficient. Thus, exactly those qualities which were expected to be the main advantage of CNS cathodes with a smooth surface over standard metal point cathodes are absent.

At the same time, the theoretical models of low-voltage emission for CNSs with smooth surfaces were formulated and extensively discussed. However, neither of these models

helped to achieve considerable progress in overcoming these disadvantages. Numerous attempts were also made to obtain the desired result by the trial-and-error method, which, however, have not resulted in cardinal success either. At present, in our opinion, it is generally accepted that the necessary condition for the successful development of field CNS cathodes with the required parameters is the careful investigation of emission mechanisms in them. Some progress in this area can be related to recent data on the features of the electron–phonon interaction in nanosize regions [145, 171–181]. These data are used in new emission models for CNSs [45, 60, 144, 157–159, 170, 173, 182, 183].

Our conclusions are presented in the table. The lines correspond to models and different carbon structures for which the given model is valid. Models considered in Section 3 were taken from the theory of field emission from metal cathodes, while those in Section 4 were specially developed to explain field emission from carbon nanostructures. The columns present experimental facts obtained in numerous studies, which should be taken into account in the construction of models of field emission from carbon nanostructures. These facts are considered in Section 2 and are again briefly formulated in the table, where they are presented by the following numbers.

Thus, the field emission from carbon nanostructures has the following properties:

(1) The existence of emission centers as regions from which the emission current comes out — small regions on the boundary with the vacuum with properties differing from the other surface.

(2) The best emission properties are inherent in strongly inhomogeneous carbon materials consisting of structural regions with drastically different (contrast) electronic and thermal properties: metal (graphite-like) and dielectric (diamond-like).

(3) Optimal conditions for emission are achieved for approximately equal proportion between graphite-like and diamond-like regions.

(4) The necessary structural element of an EC producing low-voltage emission is an isolated graphitized carbon region.

(5) The low work function of the surface or separate regions — the effective work function — is the characteristic feature of field emission from carbon nanostructures. Reports about deviations from this property of emission from carbon nanostructures require a cautious approach.

(6) The form of volt-ampere characteristics for emission from carbon nanostructures corresponds to the Fowler–Nordheim law, but can deviate from it, e.g., can have a break in the FN coordinates.

(7) The energy distribution of emitted electrons does not always contain only one peak corresponding to current according to the Fowler–Nordheim law, and can have an additional lower-energy peak.

(8) The emission process in carbon nanostructures can be inertial and can have a hysteresis.

(9) The temperatures of emitting surfaces determined from energy distributions of emitted electrons require an explanation in any model of field emission from carbon nanostructures.

The '+' sign in the table means that the given model explains this effect, and the '−' sign means that the model does not explain the effect.

Acknowledgments

E D Eidelman thanks A Ya Vul' for his attention to this study and K V Reich for his cooperation and, in particular, for his help in data processing. We thank A Yu Babenko, E F Orlenko, and N I Aleksandrov for their help in the preparation of figures, and G I Dmitrieva and N F Nechaeva for technical assistance in the preparation of the manuscript.

References

1. Fowler R H, Nordheim L *Proc. R. Soc. Lond. A* **119** 173 (1928)
2. Stratton R *Phys. Rev.* **125** 67 (1962)
3. Elinson M I, Vasil'ev G F *Avtoelektronnaya Emissiya* (Autoelectron Emission) (Moscow: Fizmatgiz, 1958)
4. Baskin L M, Lvov O I, Fursey G N *Phys. Status Solidi B* **47** 49 (1971)
5. Modinos A *Solid-State Electron.* **45** 809 (2001)
6. Chernozatonskii L A *Chem. Phys. Lett.* **233** 63 (1995)
7. Gulyaev Yu V et al. *J. Commun. Technol. Electron.* **48** 1288 (2003); *Radiotekh. Elektron.* **48** 1399 (2003)
8. Baker F S, Osborn A R, Williams J *Nature* **239** 96 (1972)
9. Sheshin E P *Struktura Poverkhnosti i Avtoemissionnye Svoistva Uglerodnykh Materialov* (Surface Structure and Autoemission Properties of Carbon Materials) (Moscow: Izd. MFTI. Fizmatkniga, 2001)
10. Gröning O et al. *Appl. Phys. Lett.* **71** 2253 (1997)
11. Obraztsov A N, Volkov A P, Pavlovskii I Yu *JETP Lett.* **68** 59 (1998); *Pis'ma Zh. Eksp. Teor. Fiz.* **68** 56 (1998)
12. Cui J B, Ristein J, Ley L *Phys. Rev. B* **60** 16135 (1999)
13. Ralchenko V et al. *Diamond Relat. Mater.* **8** 1496 (1999)
14. Karabutov A V, Frolov V D, Konov V I *Diamond Relat. Mater.* **10** 840 (2001)
15. Okotrub A V et al. *Carbon* **42** 1099 (2004)
16. Carey J D, Silva S R P *Solid-State Electron.* **45** 1017 (2001)
17. Orlanducci S et al. *J. Nanosci. Nanotechnol.* **8** 3228 (2008)
18. Koh A T T et al. *J. Appl. Phys.* **110** 034903 (2011)
19. Zhai C X et al. *Physica B* **406** 1124 (2011)
20. Nose K et al. *J. Vac. Sci. Technol. B* **30** 011204 (2012)
21. Tordjman M et al. *Appl. Phys. Lett.* **101** 173116 (2012)
22. Gupta S, Morell G, Weiner B R *J. Appl. Phys.* **95** 8314 (2004)
23. Xu N S, Ejaz Huq S *Mater. Sci. Eng. R* **48** 47 (2005)
24. Wang C et al. *Electron. Lett.* **27** 1459 (1991)
25. Obraztsov A N, Pavlovskii I Yu, Volkov A P *Tech. Phys.* **56** 87 (2001); *Zh. Tekh. Fiz.* **71** 89 (2001)
26. Gröning O et al. *Solid-State Electron.* **45** 929 (2001)
27. Krauss A R et al. *J. Appl. Phys.* **89** 2958 (2001)
28. Xu N S, Tzeng Y, Latham R V *J. Phys. D* **27** 1988 (1994)
29. Cheah L K et al. *J. Appl. Phys.* **85** 6816 (1999)
30. Rakhimov A T *Phys. Usp.* **43** 926 (2000); *Usp. Fiz. Nauk* **170** 996 (2000)
31. Zakhidov Al A et al. *J. Exp. Theor. Phys.* **97** 1240 (2003); *Zh. Eksp. Teor. Fiz.* **124** 1391 (2003)
32. Vul' A Ya, Eidelman E D, Dideikin A T, in *Synthesis, Properties, and Applications of Ultrananocrystalline Diamond. NATO Advanced Research Workshop on Synthesis, Properties and Applications of Ultrananocrystalline Diamond, 2004, Saint Petersburg, Russia* (NATO Science Ser., Ser. II, Vol. 192, Eds D M Gruen, O A Shenderova, A Ya Vul') (Dordrecht: Springer, 2005) p. 383
33. Karabutov A V et al. *J. Vac. Sci. Technol. B* **19** 965 (2001)
34. Uppireddi K, Weiner B R, Morell G *J. Appl. Phys.* **103** 104315 (2008)
35. Obraztsov A N, Kleshch V I, Smolnikova E A *Beilstein J. Nanotechnol.* **4** 493 (2013)
36. Kleshch V I et al. *Carbon* **81** 132 (2015)
37. Obraztsov A N et al. *J. Exp. Theor. Phys.* **93** 846 (2001); *Zh. Eksp. Teor. Fiz.* **120** 970 (2001)
38. Zakhidov Al A et al. *J. Exp. Theor. Phys.* **100** 89 (2005); *Zh. Eksp. Teor. Fiz.* **127** 100 (2005)
39. Kleshch V I et al. *Phys. Status Solidi B* **248** 2623 (2011)
40. Smol'nikova E A "Issledovanie strukturnykh i avtoemissionnykh kharakteristik nanografitnykh kholodnykh katodov" ("Study of structural and autoemission characteristics of nanographite cold

cathodes''), Ph.D. Thesis (Phys.-Math. Sciences) (Moscow: Lomonosov Moscow State Univ., 2015)
41. Kleshch V I et al. *Phys. Status Solidi B* **255** 1700270 (2018)
42. Arkhipov A V et al. *Tech. Phys. Lett.* **40** 1065 (2014); *Pis'ma Zh. Tekh. Fiz.* **40** (23) 58 (2014)
43. Arkhipov A V et al. *Fuller. Nanotub. Carbon Nanostruct.* **28** 286 (2020)
44. Arkhipov A V et al. *Tech. Phys.* **62** 127 (2017); *Zh. Tekh. Fiz.* **86** (12) 135 (2016)
45. Andronov A et al. *J. Vac. Sci. Technol. B* **36** 02C108 (2018)
46. Gupta S, Weiner B R, Morell G *J. Appl. Phys.* **91** 10088 (2002)
47. Fursey G N, Petrick V I, Novikov D V *Tech. Phys.* **54** 1048 (2009); *Zh. Tekh. Fiz.* **79** (7) 122 (2009)
48. Yafarov R K *Tech. Phys.* **51** 40 (2006); *Zh. Tekh. Fiz.* **76** (1) 42 (2006)
49. Yafarov R K *Tech. Phys.* **63** 126 (2018); *Zh. Tekh. Fiz.* **88** 127 (2018)
50. Davidovich M V, Yafarov R K *Tech. Phys.* **63** 274 (2018); *Zh. Tekh. Fiz.* **88** 283 (2018)
51. Pradhan D, Lin I N *ACS Appl. Mater. Interfaces* **1** 1444 (2009)
52. Karabutov A V et al. *Surf. Interface Anal.* **36** 455 (2004)
53. Arkhipov A V et al. *J. Phys. Conf. Ser.* **100** 072047 (2008)
54. Varshney D et al. *J. Appl. Phys.* **110** 044324 (2011)
55. Zhirnov V V et al. *Phys. Solid State* **46** 657 (2004); *Fiz. Tverd. Tela* **46** 641 (2004)
56. Lai S H et al. *Appl. Phys. Lett.* **85** 6248 (2004)
57. Ojima M et al. *Appl. Phys. Lett.* **88** 053103 (2006)
58. Arkhipov A et al. *J. Nanomater.* **2014** 190232 (2014)
59. Guglielmotti V et al. *Appl. Phys. Lett.* **95** 222113 (2009)
60. Vul' A et al. *Adv. Sci. Lett.* **3** 110 (2010)
61. Uppireddi K, Weiner B R, Morell G *J. Vac. Sci. Technol. B* **28** 1202 (2010)
62. Park K H, Lee S, Koh K H *J. Appl. Phys.* **99** 034303 (2006)
63. Popov E O et al. *J. Vac. Sci. Technol. B* **36** 02C106 (2018)
64. Forbes R G et al. *J. Vac. Sci. Technol. B* **22** 1222 (2004)
65. Forbes R G *J. Vac. Sci. Technol. B* **27** 1200 (2009)
66. Busta H H et al. *Solid-State Electron.* **45** 1039 (2001)
67. Ilie A et al. *J. Appl. Phys.* **88** 6002 (2000)
68. Anikin V M, Goloubentsev A F *Solid-State Electron.* **45** 865 (2001)
69. Maslov V I *Tech. Phys. Lett.* **33** 1069 (2007); *Pis'ma Zh. Tekh. Fiz.* **33** (24) 76 (2007)
70. Arkhipov A V et al. *St. Petersburg State Polytech. Univ. J. Phys. Math.* (4–2) 123 (2013)
71. Arkhipov A V ''Nizkovol'tnaya avtoelektronnaya emissiya iz nanostrukturirovannykh uglerodosoderzhashchikh materialov i pokrytii'' (''Low-voltage autoelectron emission from nanostructured carbon-containing materials and coverings''), Doctoral Dissertation, Phys.-Math. Sciences (St. Petersburg: Peter the Great St. Petersburg Polytechnic Univ., 2017)
72. Arkhipov A V et al. *Tech. Phys.* **50** 1353 (2005); *Zh. Tekh. Fiz.* **75** (10) 104 (2005)
73. Arkhipov A V, Mishin M V, Parygin I V *Surf. Interface Anal.* **39** 149 (2007)
74. Arkhipov A V, Mishin M V *Fuller. Nanotub. Carbon Nanostruct.* **19** 75 (2010)
75. Arkhipov A V, Gabdullin P G, Mishin M V *Fuller. Nanotub. Carbon Nanostruct.* **19** 86 (2010)
76. Jarvis J D et al. *J. Appl. Phys.* **108** 094322 (2010)
77. Kolos'ko A G et al. *Tech. Phys. Lett.* **39** 484 (2013); *Pis'ma Zh. Tekh. Fiz.* **39** (10) 72 (2013)
78. Cole M T et al. *IEEE Trans. Nanotechnol.* **16** 11 (2017)
79. Charbonnier F M et al. *Phys. Rev. Lett.* **13** 397 (1964)
80. Levine P H *J. Appl. Phys.* **33** 582 (1962)
81. Purcell S T et al. *Phys. Rev. Lett.* **88** 105502 (2002)
82. Reich K V, Eidelman E D, Vul' A Ya *Tech. Phys.* **52** 943 (2007); *Zh. Tekh. Fiz.* **77** (7) 123 (2007)
83. Pshenichnyuk S A, Yumaguzin Yu M *Diamond Relat. Mater.* **13** 125 (2004)
84. Fleming G M, Hengerson J E *Phys. Rev.* **59** 907 (1941)
85. Krauss A R et al. *J. Appl. Phys.* **89** 2958 (2001)
86. Schlesser R et al. *J. Appl. Phys.* **82** 5763 (1997)
87. Schlesser R et al. *Diamond Relat. Mater.* **7** 636 (1998)
88. Yamaguchi H et al. *Phys. Rev. B* **80** 165321 (2009)
89. Bandurin D A et al. *Appl. Phys. Lett.* **106** 233112 (2015)
90. Forbes R G *Solid-State Electron.* **45** 779 (2001)
91. Ahmed S F, Moon M-W, Lee K-R *Appl. Phys. Lett.* **92** 193502 (2008)
92. Ilie A et al. *Appl. Phys. Lett.* **76** 2627 (2000)
93. Carey J D et al. *J. Vac. Sci. Technol. B* **21** 1633 (2003)
94. Frolov V D et al. *Ultramicroscopy* **79** 209 (1999)
95. Cheng H-F et al. *J. Phys. Chem. C* **115** 13894 (2011)
96. Smith R C, Silva S R P *J. Appl. Phys.* **106** 014314 (2009)
97. Smith R C et al. *Appl. Phys. Lett.* **87** 013111 (2005)
98. Spindt C A *J. Appl. Phys.* **37** 3504 (1968)
99. Fursey G N et al. *Appl. Surf. Sci.* **215** 135 (2003)
100. Dyubua B Ch, Korolev A N *Elektron. Tekh. Ser. 1 SVCh-Tekh.* (1) 5 (2011)
101. Bonard J-M et al. *Carbon* **40** 1715 (2002)
102. Tolt Z L et al. *J. Vac. Sci. Technol. B* **26** 706 (2008)
103. Bonard J-M et al. *Phys. Rev. B* **67** 115406 (2003)
104. Popov E O et al. *J. Vac. Sci. Technol. B* **33** 03C109 (2015)
105. Bocharov G S, Eletskii A V *Fuller. Nanotub. Carbon Nanostruct.* **20** 444 (2012)
106. Glukhova O E et al. *Appl. Surf. Sci.* **215** 149 (2003)
107. Eletskii A V *Phys. Usp.* **53** 863 (2010); *Usp. Fiz. Nauk* **180** 897 (2010)
108. Bocharov G S, Eletskii A V *Tech. Phys.* **52** 498 (2007); *Zh. Tekh. Fiz.* **77** (4) 107 (2007)
109. Bulyarskiy S V et al. *Tech. Phys.* **63** 894 (2018); *Zh. Tekh. Fiz.* **88** 920 (2018)
110. Egorov N, Sheshin E *Field Emission Electronics* (Springer Series in Advanced Microelectronics, Vol. 60) (New York: Springer, 2017)
111. Egorov N V, Sheshin E P *J. Surf. Investig. X-Ray Synchr. Neutron Tech.* **11** 285 (2017); *Poverkhnost. Rentgen. Sinkhrotron. Neitron. Issled.* (3) 5 (2017)
112. Shen Y et al. *Adv. Electron. Mater.* **3** 1700295 (2017)
113. Katkov V L, Osipov V A *JETP Lett.* **90** 278 (2009); *Pis'ma Zh. Eksp. Teor. Fiz.* **90** 304 (2009)
114. Zhu M Y et al. *Carbon* **49** 2526 (2011)
115. Takeuchi W et al. *Appl. Phys. Lett.* **98** 123107 (2011)
116. Evlashin S A et al. *J. Vac. Sci. Technol. B* **30** 021801 (2012)
117. Qi J L et al. *J. Phys. D* **43** 055302 (2010)
118. Palnitkar U A et al. *Appl. Phys. Lett.* **97** 063102 (2010)
119. Krivchenko V A et al. *J. Appl. Phys.* **107** 014315 (2010)
120. Huang Y et al. *Carbon* **50** 2657 (2012)
121. Kokkorakis G C, Xanthakis J P *Surf. Interface Anal.* **39** 135 (2007)
122. Robertson J, Milne W *J. Non-Cryst. Solids* **227–230** 558 (1998)
123. Binh V T et al. *Solid-State Electron.* **45** 1025 (2001)
124. Vorob'ev L E et al. *Kineticheskie i Opticheskie Yavleniya v Sil'nykh Elektricheskikh Polyakh v Poluprovodnikakh i Nanostrukturakh* (Kinetic and Optical Phenomena in Strong Electric Fields in Semiconductors and Nanostructures) (Exec. Eds V I Il'in, A Ya Shik) (St. Petersburg: Nauka, 2000)
125. Forbes R G *Ultramicroscopy* **95** 1 (2003)
126. Cutler P H et al. *Appl. Surf. Sci.* **146** 126 (1999)
127. Amaratunga G A J, Silva S R P *Appl. Phys. Lett.* **68** 2529 (1996)
128. Geis M W, Twichell J C, Lyszczarz T M *J. Vac. Sci. Technol. B* **14** 2060 (1996)
129. Geis M W et al. *Appl. Phys. Lett.* **68** 2294 (1996)
130. Koenigsfeld N, Philosoph B, Kalish R *Diamond Relat. Mater.* **9** 1218 (2000)
131. Okano K et al. *Nature* **381** 140 (1996)
132. Panwar O S, Rupesinghe N, Amaratunga G A J *J. Vac. Sci. Technol. B* **26** 566 (2008)
133. Zhao W et al. *Appl. Phys. Lett.* **96** 092101 (2010)
134. Robertson J *J. Vac. Sci. Technol. B* **17** 659 (1999)
135. Baskin L M, Neittaanmäki P, Plamenevskii B A *Tech. Phys.* **55** 1793 (2010); *Zh. Tekh. Fiz.* **80** (12) 86 (2010)
136. Obraztsov A N et al., in *Electronic Properties of Synthetic Nanostructures. XVIII Intern. Winterschool/Euroconf. on Electronic Properties of Novel Materials, 6–13 March, 2004, Kirchberg, Austria* (AIP Conf. Proc., Vol. 723, Eds H Kuzmany et al.) (Melville, NY: American Institute of Physics, 2004) p. 490
137. Frolov V D et al. *Appl. Phys. A* **78** 21 (2004)
138. Carey J D et al. *Appl. Phys. Lett.* **77** 2006 (2000)
139. Xu J et al. *J. Appl. Phys.* **91** 5434 (2002)
140. Huang P-C et al. *J. Appl. Phys.* **109** 084309 (2011)
141. Arkhipov A V et al. *J. Nano- Electron. Phys.* **8** 02058 (2016)

142. Katkov V L, Osipov V A *Phys. Part. Nucl.* **41** 1027 (2010); *Fiz. Elem. Chastits At. Yadra* **41** 1916 (2010)
143. Cui J B, Robertson J, Milne W I *J. Appl. Phys.* **89** 5707 (2001)
144. Litovchenko V et al. *J. Appl. Phys.* **96** 867 (2004)
145. Reich K V, Eidelman E D *Europhys. Lett.* **85** 47007 (2009)
146. Babenko A Yu, Dideykin A T, Eidelman E D *Phys. Solid State* **51** 435 (2009); *Fiz. Tverd. Tela* **51** 410 (2009)
147. Zheng X et al. *Phys. Rev. Lett.* **92** 106803 (2004)
148. Peng J et al. *J. Appl. Phys.* **104** 014310 (2008)
149. Forbes R G *J. Vac. Sci. Technol. B* **28** C2A43 (2010)
150. Reich K V et al. *Tech. Phys.* **53** 261 (2008); *Zh. Tekh. Fiz.* **78** (2) 119 (2008)
151. Schlesser R et al. *Diamond Relat. Mater.* **7** 636 (1998)
152. Lee K-R et al. *Thin Solid Films* **290–291** 171 (1996)
153. Zhu W, Kochanski G P, Jin S *Science* **282** 1471 (1998)
154. Wächer R et al. *Diamond Relat. Mater.* **7** 687 (1998)
155. Cheng H-F et al. *Appl. Surf. Sci.* **142** 504 (1999)
156. Umehara Y et al. *Diamond Relat. Mater.* **11** 1429 (2002)
157. Dideykin A T, Eidelman E D, Vul' A Ya *Solid State Commun.* **126** 495 (2003)
158. Eydelman E D, Vul' A Ya *J. Phys. Condens. Matter* **19** 266210 (2007)
159. Eidelman E D *Tech. Phys.* **64** 1409 (2019); *Zh. Tekh. Fiz.* **89** 1491 (2019)
160. Koniakhin S V, Eidelman E D *Europhys. Lett.* **103** 37006 (2013)
161. Shakhov F M, Meilakhs A P, Eidelman E D *Tech. Phys. Lett.* **42** 252 (2016); *Pis'ma Zh. Tekh. Fiz.* **42** (5) 57 (2016)
162. Eidelman E D, Meilakhs A P *Nanosyst. Phys. Chem. Math.* **7** 919 (2016)
163. Eidelman E D et al. *J. Phys. D* **50** 464007 (2017)
164. Eidelman E D *Semiconductors* **51** 906 (2017); *Fiz. Tekh. Poluprovodn.* **51** 944 (2017)
165. Cahill D G et al. *J. Appl. Phys.* **93** 793 (2003)
166. Khalatnikov I M *An Introduction to the Theory of Superfluidity* (Cambridge, MA: Advanced Book Program, Perseus Publ., 2000); Translated from Russian: *Vvedenie v Teoriyu Sverkhtekuchesti* (Moscow: Nauka, 1965)
167. Stoner R J, Maris H J *Phys. Rev. B* **48** 16373 (1993)
168. Meilakhs A P *Phys. Solid State* **57** 148 (2015); *Fiz. Tverd. Tela* **57** 140 (2015)
169. Meilakhs A P, Eidelman E D *JETP Lett.* **100** 81 (2014); *Pis'ma Zh. Eksp. Teor. Fiz.* **100** 89 (2014)
170. Arkhipov A V et al. *Nanosyst. Phys. Chem. Math.* **9** 110 (2018)
171. Dames C, Chen G *J. Appl. Phys.* **95** 682 (2004)
172. Chen T-G et al. *Opt. Express* **18** A467 (2010)
173. Reich K V, Eidelman E D *Phys. Solid State* **53** 1704 (2011); *Fiz. Tverd. Tela* **53** 1618 (2011)
174. Zhu S et al. *Nano Res.* **8** 355 (2015)
175. Benisty H *Phys. Rev. B* **51** 13281 (1995)
176. Inoshita T, Sakaki H *Physica B* **227** 373 (1996)
177. Nozik A J *Annu. Rev. Phys. Chem.* **52** 193 (2001)
178. Pandey A, Guyot-Sionnest P *J. Phys. Chem. Lett.* **1** 45 (2010)
179. Fang H-H et al. *Nature Commun.* **9** 243 (2018)
180. Tanaka S, Matsunami M, Kimura S *Sci. Rep.* **3** 3031 (2013)
181. Li M et al. *Nature Commun.* **8** 14350 (2017)
182. Wei X et al. *Nano Lett.* **11** 734 (2011)
183. Wei X, Bando Y, Golberg D *ACS Nano* **6** 705 (2012)